UNIVERSIDAD CARLOS III DE MADRID

ESCUELA POLITECNICA SUPERIOR

IMPACT SIMULATION OF BIRD STRIKE ON SEMI-SPHERICAL TRANSPARENCIES

Application to observation bubbles in the C-295 aircraft

A Thesis submitted by Tamara Casillas Gil for the Bachelor's degree in Aerospace Engineering

---

Supervised by:
Dr Héctor Climent Máñez, Head of Structural Dynamics and Aeroelasticity, Airbus Defence and Space

June 22, 2015

Abstract

Conflicts between birds and aircraft have increased in the last years since traffic volume and bird population have spread. Although it seems an insignificant event,up to 2009, EASA sets in 242 fatalities and 90 hull losses because of these incidents and this is why Canadian customers are concerned by this increment and have demanded a specific certification for the spotter windows bubbles of C-295 aircraft. This concern has motivated the aim of this research promoted by *Airbus Defence and Space*.

The purpose of this research is the numerical simulation of bird impact on semi-spherical transparencies similar to observation bubbles in the C-295 aircraft in order to obtain a first approach of the structural behaviour under this fact.

The study is divided into three stages:

- Firstly, the characterization of the bird is performed against rigid flat metallic targets. Experimental data coming from CRAVHI project and analytical interpretation based on Willbeck's theory have been used to validate the results.

- Secondly, the characterization of the transparency is achieved, and although the lack of experimental results complicated the labour, some researches and analytical results have been used to find a suitable model.Two analyses on flat transparencies have been carried out in parallel, a monolithic transparency and a laminated model (similar to spotter windows and cabin windshields respectively).

- Finally, the semi-spherical bubble has been modelled. The explicit numerical simulation code "Visual Environment", formerly PAM-CRASH, has been used for the simulation of these impacts.

The results show the high dependence of acrylic materials on strain rates and the need to take it into consideration in the modelization of the finite element model.

Moreover, the results expressed in terms of ballistic limits show that the current spotter window monolithic design would not fail in case of a bird striking the bubble until speeds about 50 m/s, making the advantages of laminated model (in terms of weight reduction and limit speed increment) of interest for further works.

Acknowledgements

My studies has been a long journey in which much has happened and changed. I wish to express my thanks to a number of people without whom this period of my life might not have been the same and to whom I am greatly grateful.

First of all, I would like to thank to my family, specially to my parents Ricardo and Elena and my sister Natalia, for their incredible support and guidance and for making me believe that I could achieve anything that I desire.

I want to express a special word of thanks to all my friends who have shared my happiness and sadness and they were fundamental in helping me during these stressful and difficult moments. They have been a constant source of encouragement and enthusiasm.

Special mention goes to my advisor Héctor Climent Máñez, who gave me the opportunity to participate in this research and was continuously supporting me. Besides, I would express my gratitude to my colleagues of the department of *Structural Dynamics and Aeroelasticity* at Airbus Defence and Space for their help during my internship. Mainly, thanks to Juan Tomás Viana, since without its dedication this research would not have been possible.

Finally, to all the people that I have met along the way and have contributed to create the person that I am today in some way.
Thank you all.

Contents

1 Introduction **1**
- 1.1 Introduction . . . 1
  - 1.1.1 Aim of the present work . . . 1
  - 1.1.2 Background . . . 1
  - 1.1.3 History . . . 2
  - 1.1.4 Relevance of the bird strike problem . . . 3
  - 1.1.5 Airworthiness regulations on bird strike . . . 3
- 1.2 Brief literature survey of analytical and numerical methods . . . 5
- 1.3 Experimental techniques . . . 7
- 1.4 Finite Element simulation . . . 8
  - 1.4.1 The target model . . . 8
  - 1.4.2 Bird modelling methods . . . 9
- 1.5 A brief overview . . . 10

2 Rigid target **13**
- 2.1 Introduction . . . 13
- 2.2 Bird Strike Theory . . . 13
  - 2.2.1 Initial impact phase . . . 14
  - 2.2.2 Impact pressure decay . . . 15
  - 2.2.3 Steady flow regime . . . 17
  - 2.2.4 Termination of impact . . . 18
  - 2.2.5 Further considerations: porosity . . . 18
- 2.3 Characterization of the bird model . . . 19
  - 2.3.1 Numerical model for the target . . . 19
  - 2.3.2 Numerical model for the bird . . . 20
- 2.4 Sensitivity studies . . . 30
  - 2.4.1 Speed analysis . . . 30
  - 2.4.2 Energy balance analysis . . . 31
  - 2.4.3 Mass analysis . . . 32
  - 2.4.4 Inclination analysis . . . 33

3 Flat transparencies **35**
- 3.1 Transparencies: Aviation Applications . . . 35
- 3.2 Flexible target theory . . . 37
- 3.3 Flexible target definition . . . 38
  - 3.3.1 Structure definition . . . 38
  - 3.3.2 Mesh definition . . . 39
  - 3.3.3 Characterization of the material . . . 41

3.4 Numerical results and discussion 45
3.4.1 Thickness variation 45
3.4.2 Ballistic limit 48

4 Semi-spherical transparencies 55
4.1 Introduction 55
4.2 C-295 aircraft: Spotter Bubble Window 56
4.3 FEM definition of the bubble 56
4.3.1 Structure of the bubble 56
4.3.2 Boundary conditions and mesh definition 57
4.4 Semi-spherical transparency simulation 57
4.4.1 Impact location variation 58
4.4.2 Influence of curvature 59
4.4.3 Thickness variation: Ballistic limit 60

5 Further Studies And Concluding Remarks 65
5.1 Further Studies 65
5.1.1 Boundary condition definition 65
5.1.2 Temperature effect 66
5.1.3 New Observation bubble design 67
5.1.4 Test validation 67
5.2 Concluding Remarks 67

Appendices 69

A Project Budget 71

B Validation tests budget 73

C Rigid Target Results 75

List of Figures

1.1 Most likely damaged aircraft zones [6] 4

2.1 Initial phase [17] 15
2.2 Impact pressure decay [17] 15
2.3 Variation of critical length with impact velocity for water 16
2.4 Steady flow phase [17] 17
2.5 Termination phase[17] 18
2.6 Effect of porosity for water 19
2.7 Location of pressure gauges (dimensions are mm) 21
2.8 Birds techniques 22
2.9 B-spline [7] 22
2.10 Particles displacements of both Lagrangian technique at different times 23
2.11 Particles displacements of SPH technique at different times . . . 23
2.12 Shapes of the projectile 23
2.13 Variation of shape 24
2.14 Duration analysis varying shape's bird 25
2.15 Pressure analysis varying shape's bird 25
2.16 CPU time analysis varying shape's bird 26
2.17 Different configurations of SPH particles 27
2.18 Comparison of configurations in terms of duration 28
2.19 CPU time of configurations A and B 28
2.20 Pressure analysis for both configurations 29
2.21 Particles displacements of with default viscosity ($\alpha = 0.04$ and $\beta = 0.01$) SPH technique at different times 29
2.22 Particles displacements with 1.5 viscosity values at different times 29
2.23 Comparison of configurations 30
2.24 Porosity analysis 31
2.25 Kinetic energy analysis 32
2.26 Mass variation 33
2.27 Contact force varying mass 34
2.28 Hugoniot Pressure vs. Incident angle 34

3.1 Examples of bird collisions 36
3.2 Elastic target during early shock wave[3] 37
3.3 PMMA piece after impact by spherical projectile at v=100 m/s[25] 39
3.4 Behaviour oh PMMA after impact[25] 40
3.5 Mesh process 40

3.6 Stress vs. Strain curves at different strain rates 43
3.7 Strain rates: numerical behaviour using Material type 143 44
3.8 Makeup of two-ply laminated glass and an equivalent monolithic material 46
3.9 Maximum pressure vs. velocity 47
3.10 Ballistic limit of flat transparencies 49
3.11 Collapse sequence for monolithic case (t=5 mm) at 50 m/s . . . 50
3.12 Collapse sequence for monolithic case at (t=5 mm) 150 m/s . . . 51
3.13 Collapse sequence for monolithic case (t=5 mm) at 50 m/s (Isometric view) 52
3.14 Collapse sequence for monolithic case (t=5 mm)at 150 m/s(Isometric view) 53

4.1 Observation bubble.C-295 Persuader[6] 55
4.2 Configuration of C-295 aircraft[32] 56
4.3 Observer Window FEM 57
4.4 Observer Window FEM star pattern (t=8 mm at V=75 m/s) . . 58
4.5 FEM bubble: Position's variation 58
4.6 Position's variation:Ballistic limit 59
4.7 Ballistic limit comparison between flat and semi-spherical transparencies 60
4.8 Ballistic limit: variation of thickness 60
4.9 Collapse sequence for monolithic bubble (t=5 mm) at 25 m/s . . 61
4.10 Collapse sequence for monolithic bubble (t=5 mm) at 25 m/s (Isometric view) 62
4.11 Collapse sequence for monolithic bubble (t=5 mm) at 150 m/s . 63
4.12 Collapse sequence for monolithic bubble (t=5 mm) at 150 m/s (Isometric view) 64

5.1 C-shaped frame[33] 66

C.1 Variation of shape: pressure 75
C.2 Configurations' pressures 76

List of Tables

2.1 Parameters of the rigid plate 20
2.2 Parameters of bird techniques 21
2.3 Bird shapes parameters 24
2.4 Configurations A and B parameters 27
2.5 Parameters of bird selected 30

3.1 Material type 126: material properties 45
3.2 Thickness and mass properties 47

A.1 Project phases 72
A.2 Equipment and software licenses costs 72
A.3 Project Budget 72

B.1 Experimental project phases 74
B.2 Equipment costs 74
B.3 Bird strike performance costs 74
B.4 Project Budget 74

Chapter 1

Introduction

"Begin at the beginning, the King said gravely, and go on till you come to the end: then stop."

- Lewis Carroll, *Alice in Wonderland*

1.1 Introduction

1.1.1 Aim of the present work

Transparencies are a critical component of all aircraft. They must provide a good visibility and at the same time be safe and fulfil all the requirements. However, this has become a complicated issue, since structural behaviour is critical and reduction of weight is always a point to take into account. Therefore, bird strikes are threats that can cause significant damage and this is why they are crucial object of study in the aviation field.

The objective of this research was to make a study of different bird strikes on semi-spherical transparencies similar to observation bubbles in the C-295 aircraft, which has not been already studied. This project was proposed as a first approach to fulfil the demand of Canadian customers who are concerned about the growth of Canada geese population and the number of bird strikes over the world

These analyses were done with the help of a finite element analysis making a simulation of bird strikes.

1.1.2 Background

Birds and aircraft coexist in the same airspace, which implies a huge trouble in aviation, since a bird strike incident is one of the most dangerous threats. As engineering has evolved, the number of aircraft flying has increased and their capabilities, as the speed of flight, have improved. To this fact, it must be added the growth of bird population [1], leading to a damage increment due to these events over the years.

A bird strike is defined as a collision between an airborne animal (usually a bird) and a man-made vehicle, especially aircraft. This is one of the major

hazards for flight safety and is very common throughout the world at all airports and along aircraft flight routes.[2]

Due to the relevance of this problem, several investigations have been carried out, but the problem is not completely solved. The actions taken by airworthiness regulations have reduced the hazard to the aircraft due to a bird strike, but it is not eliminated. Hence, every component of aircraft needs to have the capacity to resist any impact without damaging the primary structure. For this purpose, a full understanding of the event, the loads generated in such collisions and the response of the structure is required. In order to solve these kind of problems and study them, different numerical techniques have been developed. These tools provide huge benefits since they can help to have a deeper understanding of the problem.[3]

1.1.3 History

Birds and aircraft conflict has existed since the first flights. The first incident with a bird, exactly with a red-winged blackbird, occurred the 17 September 1905, reported by one of the Wright Brothers.

In 1911, Eugene Gilbert, who flew an open-cockpit aircraft, found an eagle during an aviation race. He was able to parry the bird and no consequences took place.

It was on 3 April 1912 when the first death as a consequence of a bird strike occurred. This was Calbraith Rodgers, the first person who flew across USA, and the fact was due to the collision of the aircraft with a gull in California.

But, the first huge loss of life due to a bird strike was on October 4, 1960. A collision of a Lockheed L-188 Electra with birds during take-off from the airport of Boston Logan occurred. The four engines stalled and the plane crashed with 62 fatalities out of 72 passengers. Then, FAA[1] developed standards concerning bird strikes for jet engines.

In 1964, a fatal crash with a goose killed Theodore Freeman, a NASA astronaut. And in 1988, 35 passengers were killed because pigeons were absorbed by the engines of Ethiopian Airlines Flight 604.

1995 was a fateful year, ten people died after an emergency landing of a Dassault Falcon 20 because of an engine failure after sucking lapwings. In this same year, a Boeing E-3 Sentry crashed killing 24 people due to the ingestion in the engines of several Canada geese during take-off.

Although the 21st century is the century of innovation and development, it has already witness birds strikes accidents. Starting with the accident of a Boeing 737-400 happened on November 28, 2004, due to a broken cable in the nose wheel because of a bird collision. None died but the aircraft was written off.

On July 26, 2005, the Space Shuttle Discovery hit a vulture during launch without important consequences.

In 2007, a Boeing 757 was able to evacuate safely all crew without incident after a bird strike. One year later, in 2008 an emergency evacuation was performed because of the failure of both engines of a Boeing 737-8AS due to another impact with a bird. Passengers were evacuated safely although the landing gear was broken after touchdown.

[1] FAA: Federal Aviation Administration

On January 2009 two facts relating with a bird strike occurred: 8 of 9 people flying in a Sirosky S-76 helicopter died because a hawk hit the windscreen. And in this same month, a successful water landing of an Airbus A320 in the Hudson River after multiple bird strike, exactly a flock of geese at 3200 ft, was performed causing just some injuries on the occupants and crew.

One of the most recent events was on September 28, 2012 in Nepal where a Sita Air Dornier Do 228 crashed with a vulture after taking off. Sixteen passengers and three crew members died.

With the evolution of aviation, the purpose of aircraft design has been to reduce the damage caused by those kind of impacts. However, as the bird population and air traffic have increased, the problems are still not totally solved.[2]

Summing up, up to 2009 EASA has set the total number of bird strike incidents to 47 in commercial air transport causing 242 fatalities and 90 hull losses [1]. Although in the IBSC meeting in 2012, it was now set to 55 accidents and 276 fatalities [4] up to 2012. Therefore, it is obvious that an effort must be done to try to avoid these kind of incidents.

1.1.4 Relevance of the bird strike problem

Bird strikes are not common accidents, but they can produce significant damage.

From all studies made, it has been identified that the highest rates of reported bird strikes (186 per million flying hours) were to CS-25 this is large aeroplanes, while CS-27, i.e. small rotorcraft, have the highest proportion of strikes resulting in damage (49% of all accidents), predominately windshields.[1]

All bird strike accidents have been directly related with high kinetic energy, meaning heavy birds and high speed. This is the reason why, although it is estimated that about 95% of strikes occur during take-off, climb, approach and landing (i.e. low altitudes), the damage produced at altitudes above 2000 ft is about 67% more harmful, due to the speed increment [1]. To this, it must be added that the typical weight of birds varies between 4 lb (1.8 kg) and 8 lb (3.6 kg), corresponding to vultures and Canada geese respectively.

During the last decade, a new and serious threat has become evident due to the increasing number of Canada Geese. This has concerned the authorities because the combination of air traffic growth and the goose population increment will produce a substantial increase of risk unless positive action is taken.[5]

In financial terms, bird strikes cause significant economic loss, about 1 billion worldwide every year.

Events show that the most likely damaged components are leading edges of wings (22%) and tails (5%), engines (35%), noses (7%) and fuselage (11%).[2] However due to the location of windshields, the study of bird impacts in this part of the structure must be primordial for aircraft and crew safety, in spite of the fact that it only represents a 5% of the whole bird strikes.[7]

1.1.5 Airworthiness regulations on bird strike

A safe aviation must be ensured through procedures and programs, and in order to provide them, regulations are established and enforced. There are two

[2]Percentages represent an estimation of the amount of bird strike in each component.

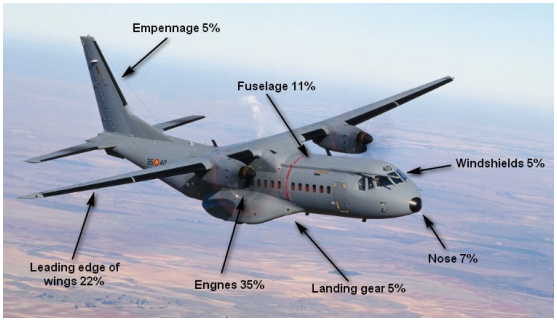

Figure 1.1: Most likely damaged aircraft zones [6]

agencies which are in charge of it: EASA (European Aviation Safety Agency) and FAA.[8]

EASA is the aviation authority of the European Union, while FAA is the aviation authority of United States. However, both work closely to have the best aviation practice worldwide balancing standards.

Concerning bird strikes, both agencies provide a set of requirements to be fulfilled. As the aircraft of interest for this analysis a C295 aircraft, the regulations to be taken into account correspond to the section CS-25 of EASA (Large airplanes) and FAR-25 of FAA (Airworthiness Standards: transport category airplanes). Finally, due to its military character,the UK DEF-STAN is the third applicable regulation that can be taken into consideration.

CS 25.631 requires that an airplane must be designed in order to ensure the capability of continued safe flight and landing of the airplane after impact with a 4 lb bird when the velocity of the airplane (relative to the bird along the airplane's flight path) is equal to Vc, cruise speed, at sea level or 0.85 Vc at 8000 ft, whichever is the more critical. Compliance may be shown through analyses only when based on tests carried out on sufficiently representative structures of similar design. The phrase "continued safe flight and landing" may be interpreted in different ways and the effects of bird strike are also addressed in various other sections of CS-25. However, bird strikes are taken into account in other sections of the regulation:

(a) CS 25.571(e): no fail can be produced during the complete flight which likely structural damage occurs as a result of bird impact as specified in CS 25.631;

(b) CS 25.629 which states that the airplane must be free from aeroelastic instability for the configuration of CS 25.629 (b)(2);

(c) CS 25.775(b) requires windshield panes directly in front of the pilots in the normal conduct of their duties, and the supporting structures for these panes, must withstand, without penetration, the bird impact conditions specified in CS 25.631. In addition, CS 25.775(c) says that "unless it can be shown by analyses or tests that the probability of occurrence of a critical windshield fragmentation condition is of a low order, the airplane must have means to minimize the danger to the pilots from flying windshield fragments due to bird impact";

(d) CS 25.1323(j) which requires that "where duplicate airspeed indicators are required, their respective Pitot tubes must be far enough apart to avoid damage to both tubes in a collision with a bird";

(e) AMC 25.631 stipulates about the location and installation of items which are essential services, i.e. which could produce a hazard if they are damaged because of a bird strike;[3]

(f) AMC 25.1309(b) where bird strike is identified as a Particular Risk, defined as those events which are outside of the systems concerned, requiring investigation as part of the Common Cause Analysis.[9]

FAR regulations are similar to the previous ones, and for each of these regulations, there is another one which fits exactly with the one stated by EASA:

(a) FAR 25.571(d)(1) requires the same than CS 25.631;

(b) FAR 25.629(b) is identified with CS 25.629;

(c) FAR 25.775(b)&(c) "Windshield and windows" fits exactly with CS 25.775(b)&(c);

(d) FAR 25.132(j) "Airspeed indicating system", stating the same than CS 25.1323(j);

(e) FAR 25.773(b)(4)(ii) which requires that the openable window of the pilot must remain sufficiently clear for at least one pilot to land safely in the event of an encounter with several birds.[8]

However regarding empennage, FAR states that the aircraft must be able to widhstand a bird strike of 8 lb at cruise speed (FAR 25.631) while the CS-25 just requires a 4 lb bird.

Finally, the last Applicable regulation extracted from DEF-STAN 00-97: Volume 1, chapter 209 states that: "the effect of a single defined bird strike shall not degrade flying qualities below level 2[4]". Consideration shall be given to minimize the cost of repairing bird strikes in defined areas. Acceptable reparability shall be demonstrated. The maximum threat is a 1.0 kg bird at V_M, manoeuvring speed, (but>480 Kt TAS). Defined locations are frontal aspects of windscreen and forward facing transparencies.[10]

In addition, for transparencies at V_M no serious cracking or delaminating can appear, not generate debris, and it must be acceptable optical qualities. And at 1.1 V_M no penetrations are allowed.[7]

1.2 Brief literature survey of analytical and numerical methods

In the 1960's, several English people investigated the deflection of beams due to the impact of soft objects. Tudor developed a relationship between beam

[3]AMC stands for Acceptable Means of Compliance.

[4]Levels of flying qualities makes reference to the ability to complete the operational missions for which the aircraft is designed. Level 2 has to accomplish the mission flight phase, but with increase in pilot workload or/and degradation in mission effectiveness.

deflection and initial momentum of the projectile and MacCauley and Mitchell [3] elaborated a theoretical study of bird loading which provided a first approach to the real impact without experimental checks.

For the impact of solids, it was Hopkins and Kolsky [3] who divided the impact into five physical regimes: elastic, plastic, hydrodynamic, impact at sonic velocities and explosive impacts. Although these regimes were defined for low strength projectiles, it is assumed their validation for high strength projectiles.

Hopkinson [3] found experimentally that the stress in a rigid target (steel) was similar to the expected from a fluid jet. He arrived to the conclusion that high-strength materials "flow" if they are subjected to very high pressures. Consequently, a further research in this field was required.

Heymann [3], after focusing on water jets and water droplets, stated several features of impact process, as the area over which pressure acts, the initial impact pressure, the velocity of the lateral outflow of liquid and the approximate decay time of high impact forces. Then, Heymann [3] and the preliminary work of Cook in 1928 identified the two basic regimes of water jet impact: the initial shock regime and the late-time steady flow regime.

Later, Jenkins and Booker agreed with Bowden and Field [11] explaining that the maximum impact pressure is the Hugoniot pressure and it is uniform until lateral jetting begins.

Due to the disagreement over the amplitude, distribution of peak pressures and lateral flow velocities, an effort was carried out to improve experimental techniques in order to understand the impact event. Then, it was in 1975 when Barbers, Taylor and Willbeck [11] developed the bird-strike theory as a soft body impact problem. They studied the bird impact against a rigid target in order to characterize this kind of strikes, obtaining an acceptable theory.

Concerning the characterization of bird impacts through non-linear finite element codes, over the years, several ones have been implemented, such as MAGNA, MARC, NONSAP-M, DYNA3-D, PAM-CRASH, ABAQUS, MSC-DYTRAN or LS-DYNA. All these codes have differences as a function of their sophistication.

Niering [12] modeled the bird shape using DYNA 3-D. He found that Hugoniot pressure might produce initial damage and reduction of strength. Then, Vasko [12] implemented the Lagrangian approach using LS-Dyna in a fan blade impact, modelling the bird as an ellipsoid of solid elements. This simulation was compared with experimental results.

Hörmann et al. [12] selected the Lagrangian and Arbitrary Lagrangian Eulerian (ALE) technique for the characterization of the bird. The bird was shaped as a cylinder with hemi-spherical ends. Different behaviour of the bird was observed depending on the technique developed.

A Smoothed Particle Hydrodynamcis (SPH) model was used by Anghileri et al. The comparison with experimental results was in agreement with the ones obtained with LS-Dyna. Anghileri [12] was able to improve some characteristics of the model thanks to the experimental results validation. Besides, the usage of all available techniques was implemented, concluding that SPH particles provide the most suitable results.

1.3 Experimental techniques

In order to validate the numerical and analytical results it is needed to perform experimental results. They provide the measurements of the different results of forces and pressures generated during the impact.

These experimental tests are composed of an impactor or projectile, a launcher, a target and several measurement instruments:

- The impactor or projectile: it is a bird. One of the main problems of the execution of experiments with birds is that the composition of each bird is not always the same because of its non-homogeneity. Consequently, it is very difficult to validate the results, since it is impossible to obtain exactly the same output, but the results ensure statistical representativeness. Hence, real birds are actually used for testing. They must be alive and the test must be in accordance to FAR 25 and CS-25 previously described in 1.1.5, this is why birds used weights 1 kg, 4 lb (1.81 kg) and 8 lb (3.62 kg).

- The launcher is usually a cannon or gun. It launches the bird at a defined velocity and orientation and it should be designed to keep the impactor (bird) intact. Inside this device, the projectile, i.e. the bird, is placed in a sabot. A sabot is a cylindrical open-ended carrier that seals the gun and it is removed from the bird before impact since it adds mass which disturbs the result.

- The target is the object where the projectile is going to impact. There are two typical targets, the rigid and the flexible. Rigid targets are focused on the characterization of the bird, since the target has not influence on the results. However, typical real structures are not completely rigid, this is why flexible target are used to represent them in a more realistic way.

- Measurement equipment is required to obtain data from the test and typical equipment is composed of strain gauges, pressure transducers, accelerometers or high speed cameras. Strain gauges measure impulse during the impact and pressure transducers measure the temporal distribution of pressure at different points of the target [3]. Accelerometers are used to record stress waves and vibrations caused by a bird strike although the connection using cables can resulted in shorts causing outages. And finally high speed cameras provide the collapse sequence allowing the observation of the behaviour of the bird during the strike.

Regarding available tests, it can be divided into different tests depending on the section of study:

- Windshields: in order to ensure the safety of the pilot and the aircraft must be accomplished. This test has to show that the target, the windshield, is able to withstand the impact. In the last years new technology has been implemented to obtain more detailed information of each strike. High speed cameras are employed from which data as sabot fragments, fluid behaviour of the bird, amplitude waves or deflections of the target can be extracted for further investigations.

- Leading edges: wing shots are performed to studying them. These tests check that birds do not penetrate leading edges and that any part, such that spars or full cells, are damaged.
- Empennage: in a similar way than leading edges, empennage strikes are tested to analyse the vulnerabilities of the vertical fin and horizontal stabilizer, where the spars cannot be damaged, broken or fractured.
- Engine: engine shots are examined to prove that after an impact, the engine is capable to produce at least 75% thrust for 5 minutes and the fan disk maintains its integrity (in accordance to FAR 25 and CS 25).[12]

However, the main problem of all these tests is the cost. They are quite expensive and it is not easy to repeat them with the same accuracy. This is why numerical simulation has become essential to perform a first approach and a preliminary study of the design to improve it before testing. In that sense, numerical simulations are nowadays very attractive due to the high possibilities that they offer, although much more remains to be done in this field.

1.4 Finite Element simulation

In the late 70's, the US Air Force was the pioneer of adopting the finite element method (FEM) as a bird strike analysis tool. However, due to the complexity of bird strike, the accuracy of the first linear FEM results was about 50%, being not acceptable. The introduction of non-linear codes improved the results since geometrical and material non-linearities were taken into account, although the initial pressure and tangential forces were neglected. Some of those codes were NONSAP, DYNA3D, BASIS, BINA or PAM-CRASH.[13]

For the purpose of this study, the "Visual Performance solution" usually called PAM-CRASH (version 2010) tool was used. PAMCRASH is a general purpose explicit finite element computer program for non-linear dynamic analysis of structures in three dimensions. PAMCRASH is integrated into the PAMSOLID library of solvers.[14] This is a software package from ESI Group.

The numerical simulation of the bird-strike test is carried out using the explicit finite element technique. The Finite Element model created consists mainly of two parts: the bird and the target.

1.4.1 The target model

The target in this research is a numerical simulation of the observation bubble of C-295 aircraft. It is modelled as a semi-spherical bubble and in order to achieve this objective, some previous work needs to be done.

First of all, the target is represented as a rigid in order to study the bird model and check the results obtained. After that, transparencies are created for which different materials of PAM-CRASH are investigated. Finally, the definitive structure will be created and studied.

The principal characteristics to be taken into account are:

- **Geometry**: this feature is varying through the core of the work until the final geometry is implemented, in order to verify and validate results. It is fateful to defined correctly and precisely to avoid any possible error.

- **Mesh**: it has to be discretized in a determined number of nodes, such that it provides an accurate result taking into account the time spent.
- **Material selection**: this point is very important to ensure a realistic result. PAM-CRASH has hundreds of different materials and it is needed to choose it carefully. Its properties and the thickness of the model determine the weight, which is a very important point to take heed of.
- **Boundary conditions (B.C)**: They are imposed, and they simulate the points of links with the fuselage.It is important to take care of the B.C definition, a wrong B.C. representation can have some influence on simulation results.

1.4.2 Bird modelling methods

Although the modelling of soft bodies is still under research nowadays, there are several accurate techniques to simulate them. Three different FE models were developed: a Lagrangian model, a Smoothed Particle Hydrodynamics (SPH) model and an Arbitrary Lagrangian-Eulerian (ALE) model.[15]

Lagrangian bird impactor

The Lagrangian method uses material coordinates as reference, i.e. the mesh nodes are associated to the material and consequently they move as the material does. The boundary of the body is clearly defined because the nodes always remain in the material boundary, simplifying the boundary condition. This model, which is normally used for solid materials, has clear advantages and disadvantages. The advantages are that it spends less CPU time compared with other approaches because the time step decreases, and as it has been already mentioned, the boundary conditions are easily defined.

On the other hand, mesh deformations cause inaccurate results. Two solutions exist for this problem: remeshing the region of mesh tangling, although this provokes an increase of the numerical errors and the cost. The second solution consists of deleting the distorted elements; this technique is called element erosion. As a consequence, artificial oscillations and a decrease in the mass appear, but they can be solved by using fine meshes and by lumping the mass to the nodes respectively.[13]

Arbitrary Lagrangian Eulerian (ALE) bird impactor model

This model was created with the purpose of reducing the high distortion problems of the Lagrangian model, so to solve it, the model uses a mixture of the Lagrangian and Eulerian techniques.

The nodes and mesh of the Arbitrary Lagrangian Eulerian (ALE) model are fixed in the space and the material flows through the mesh. Then, the distortion is impossible because of its restraint, avoiding the Lagrangian problem [15]. However, ALE shows some disadvantages: the definition of the boundary depends on the mesh size, and the cost is higher than the Lagrangian one. The domain for computational analysis is larger since it must cover the area where the material exists in the present instant and the area where it can exist later in the simulation. Besides, the cost increases due to the higher number of elements

and iterations performed, and consequently, longer time of CPU computation is consumed. Dissipation and dispersion problems are another characteristics of this approach, coming from the interchange of mass of the elements. Finally, as ALE results depend significantly on the mesh, it requires fine meshes and the accuracy is not one of its virtues.[13]

Smooth Particle -hydrodynamics (SPH) impactor bird

This approach is a meshless technique composed by a set of particles. Each particle is independent of the others, moves according to the conservation equations and has individual mass and velocity properties. Due to this absence of grid, this model has a lot of advantages:

There are not problems with irregular geometries and mesh distortion since no grid is needed. Other advantage is the fewer number of elements required by SPH in comparison with the Eulerian model; due to this reason the CPU time is reduced without affecting the results, although it spends more time than the Lagrangian. Moreover, SPH has good stability and it can be split into several parts being able to pass through small holes.[7]

On the other hand, some disadvantages are carried out by this approach: larger computer memory is required, the boundary condition is not easily defined, as well as the relationship between the fluid and the structure and finally, the impact area is not defined since SPH has not a trace.[16]

1.5 A brief overview

The present project is divided into five chapters, each of them is focused on one specific aspect of the analysis. The structure and contents of each one are listed below:

- The present chapter makes a global vision of the problem, analysing its relevance, and documenting the history of bird strikes and accidents as the current airworthiness regulation. With the aim of gaining an understanding on the fundamentals and state of the art of the area, a literature survey is provided in this same chapter. Furthermore, the different kinds of numerical simulation are introduced doing a comparative analysis between them.

- In chapter 2, the bird modelling in explicit Finite Element is implemented doing a characterization of the bird. For that purpose, a sensitive analysis of the numerical simulation of bird strike against rigid flat surfaces is performed correlating different information with experimental test results.

- The chapter 3 is focused on the characterization of flat transparencies and the numerical simulations of bird strikes in such surfaces. Different analyses varying the angle of impact of the projectile in the target surface, the mass, the velocity have been accomplished. And as a final point, after the comparison of the results with published test data-set, the modelization of a transparency is obtained.

- In chapter four, the study is the backbone of the project since the characterization of “observation bubbles” is executed. This numerical

simulation is based in the bird strike on the observation bubble of the C-295 aircraft. An investigation similar to the one of chapter 3 is done for this case. Here, the different decisions are explained in detail in order to find the best solution that fits the system.

- The last chapter wraps up the work performed, showing the final results and conclusions. In addition, some design guidelines and recommendations are given with some proposal of future activities.

- Finally, a supplementary material is provided at the end of the project. Extra pressure data of rigid target tests is given and moreover a budget estimation of the project and the budget required to validate numerical results in a future are presented.

Chapter 2

Rigid target

"Failure will never overtake me if my determination to succeed is strong enough."

- Og Mandino,

2.1 Introduction

The first step in this research is the characterization and validation of the projectile, the bird.

This is crucial for the aim of the thesis in order to obtain good results for the transparencies simulations, for which experimental data is not available (only comparison with some results published in literature is established).

A detailed study to find which are the characteristics of the bird that better fit the experimental data is carried out: first of all, theoretical results are computed, then the model is created using PAM-CRASH, and finally the results are validated with experimental data.

For this purpose, the experimental data used in this study comes from the real tests within CRAVHI (CEAT and Airbus UK info) [9]. The CRAVHI (Crashworthiness of Aircraft for High Velocity Impact) project was a long program regarding the structural resistance of aircraft to extreme situations as crashes or impacts. The motivation of this project was to improve the safety of the aircraft under emergency situations.[1]

Following sections show a detailed study of the numerical, analytical and experimental data, finally obtaining the definitive bird which will be used for the whole project.

2.2 Bird Strike Theory

In the present section, a theoretical description of the bird impact was undertaken, in order to understand the process. This theoretical analysis is not absolutely rigorous, since a lot of factors enter into this complex process

[1] It must be noted that CRAVHI tests were done with real and synthetic birds, but in this analysis only the real ones are taken into consideration.

and it is not easy to represent. However, this is a guidance of the experiments and data reduction process.[17]

First of all, the simplest approach is elaborated in which a cylinder impacts into a rigid target. After that, several modifications are put in: projectile with a curved leading edge, inclination of the projectile or addition of porosity to the projectile material.

Concepts from various disciplines are integrated to develop a reliable impact theory. An impact can be classified in three different ways [17]:

- **Elastic impact**: in this case velocity is usually low and the stresses generated after the collision are lower than σ_y. Consequently, the time spent on the impact depends on the elastic modulus and the elastic wave velocities.

- **Plastic impact**: this is the opposite case than the elastic impact. In plastic impacts the velocity is very high, then the material factor is the critical one since the stresses after the impact produce plastic deformations.

- **Hydrodynamic impact**: higher impact velocities occur in this type. The projectile is treated like a fluid and the stresses are larger than σ_y because of the deceleration of the projectile. In this impact, the dominating factors are the mass, the density of the material and the speed of the projectile, not its material strength.

Bird strikes belong to the last kind of impacts, the hydrodynamic ones, since in a bird impact the bird behaves as a "soft body". Peterson and Baber [3] stated that birds behave like a fluid during an impact.

Therefore, the process is divided into four phases or stages, in which a homogeneous right circular cylinder impacting normally on a rigid plate is considered and explained right after:

- Initial impact phase
- Impact pressure decay
- Steady flow regime
- Termination of impact

2.2.1 Initial impact phase

When the bird impacts the rigid target, the front face of the impactor curve comes to rest and a shock wave propagates into the bird as it is depicted in figure 2.1. The flow across a shock can be considered as one-dimensional, irreversible and adiabatic. Then, the conservation laws, mass and momentum across the shock are stated taken the steady shock condition:

$$\rho_1 u_s = \rho_2 (u_s - u_p) \tag{2.1}$$

$$P_1 + \rho_1 u_s^2 = P_2 + \rho_2 (u_s - u_p)^2 \tag{2.2}$$

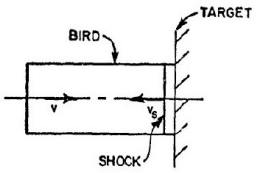

Figure 2.1: Initial phase [17]

Where u_s stands as the velocity of shock wave propagating and u_p as the particle velocity behind the shock wave. Combining equations (2.1) and (2.2), the pressure behind the shock, namely Hugoniot pressure, is:

$$P_H = \rho_1 u_s u_p \tag{2.3}$$

It must be remarked that for the Hugoniot, u_p=u_o where u_o stands by the projectile's initial velocity:

$$P_H = \rho_1 u_s u_o \tag{2.4}$$

and at low impact velocities (compared with the sound speed in the bird material), u_s is approximately equal to the isentropic sound speed of the material c_o:

$$P_H = \rho_1 c_o u_o \tag{2.5}$$

Notice that the particle velocity is the change in velocity across the shock and this pressure is very high and uniform in the compressed area.

For the oblique impact of a projectile in a rigid plate, some settings must be applied in order to ameliorate the result. For that purpose, equation (2.4) is modified into:

$$P_H = \rho_1 u_s u_o sin\theta \tag{2.6}$$

where θ represents the angle at which the bird impacts.

This stage will finish when the release wave, composed from the radial acceleration of the particles because of the compression gradient, arrives to the center of the bird. Then, the decay stage starts.

2.2.2 Impact pressure decay

The problem cannot be longer treated as a one-dimensional problem, since the shock wave begins to propagate longitudinally into the projectile and the release waves move radially towards the center of the projectile, transforming into a 2D symmetric problem. It is illustrated in figure 2.2.

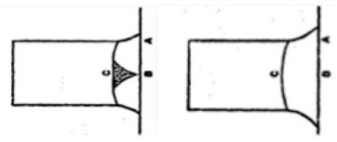

Figure 2.2: Impact pressure decay [17]

Figure 2.2 shows that the pressure at point "B" is given by equation (2.3), but once the pressure starts to decay, the fully shocked region no longer exists.

The shock curvature observed is produced due to the release process, which has progressively weakened the shock.

In this stage, two interesting parameters can be computed: the time required by the released wave to reach the bird center, given by equation (2.7), and the critical projectile length.

$$t_r = a/c_r \tag{2.7}$$

The equation (2.7), where "a" stands by the cylinder radius and "c_r" is the speed of sound in the shocked material, gives a first approach to calculate when the pressure starts to decay.

Concerning the critical length (l_c), it comes from the relation showed in equation (2.8)

$$(l/d)_c = \frac{u_s}{2\sqrt{(c_r^2 - (u_s - u)^2)}} \tag{2.8}$$

Where "d" the diameter of the projectile.

The ratio l/d is very important in order to define the geometry of the projectile:[17]

- If $l/d > (l/d)_c$,the shock wave is weakened because the reflected waves reach it and the shock wave effect will be reduced or even eliminated before reaching the projectile rear surface.
- If $l/d < (l/d)_c$ the projectile experiences a shock wave decay to steady flow since the reflected shock wave does not reach the longitudinal shock waves. As consequence, the end of the bird is reached without getting weaker. This rarefaction wave could complicate the impact provoking the projectile failure.

Typical values for a bird of null porosity (this is water) is depicted in figure 2.3

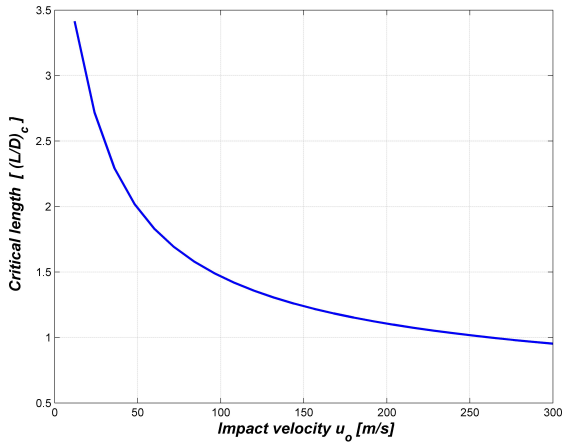

Figure 2.3: Variation of critical length with impact velocity for water

Finally, the radial pressure distribution can be calculated from the following equation:

$$P_r = P_c e^{-\sqrt{\frac{Kr}{R(t)}}} \tag{2.9}$$

P_c is the pressure at the center of the impact zone, K is a constant, r is the radial distance from the center and R(t) is the maximum contact time radius at each time. It is obvious that the pressure decreases as the the distance from the center increases.[12]

2.2.3 Steady flow regime

As shock velocity decreases in the release phase, the shock will be weakened until it disappears, if it is subsonic. In the contrary, for the supersonic case, it does not disappear, as the velocity will decrease until a standing shock is created. After that, the shock becomes subsonic and it will follow steady state streamlines.

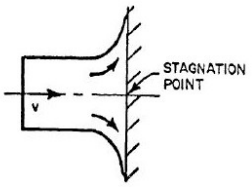

Figure 2.4: Steady flow phase [17]

This analysis is focused on the subsonic condition, where the experimental results have provided an analytical solution for the pressure called stagnation pressure, P_s:

$$P_s = k\rho_o u_o^2 \tag{2.10}$$

This pressure is the one generated in the center of the impact, where an stagnation point is located. It is deduced from equation (2.10) that P_s does not depend on the bird shape similar to P_H. However, the transition between P_H and P_s will depend on the shape of the bird.

For an incompressible fluid, the constant k is 1/2; however, for other materials, since density is proportional to pressure, the value of k goes to 1.

In the same line of thought, from the impulse equation, the force generated in this steady flow regime and the duration of this stage are obtained:

$$F = \rho A u_o^2 \tag{2.11}$$

$$t_D = L/u_o \tag{2.12}$$

being L the initial length of the projectile.

To end up, Leach and Walker stated a expression to predict the steady radial pressure distribution due to normal impact for soft body impacts:

$$P = P_s(1 - 3\left(\frac{r}{\tau a}\right)^2 + \left(\frac{r}{\tau a}\right)^3 \tag{2.13}$$

Where r is the radial distance from the center, a is the initial radius of the bird and τ is given by equation (2.14).

$$\tau = (3.33 P u_o^2)/P_s)^{1/3} \tag{2.14}$$

However, the relation (2.13) does not take into account the compressibility effects, being only valid for incompressible cases.[3]

2.2.4 Termination of impact

The last period is the flow termination. As the fluid nears the target surface, the velocity decreases and consequently, the local pressure increases. At the end, when the projectile enters completely into the pressure field, the field is obstructed due to the free surface of the projectile. Pressure decreases and the steady flow vanishes.

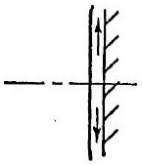

Figure 2.5: Termination phase[17]

The total time of the strike can be approximated by equation (2.12) since in proportion, the steady flow phases are much longer than any of the other.

2.2.5 Further considerations: porosity

After an accurate study of bird's composition was carried out, Willbeck concluded that the modelling of a bird cannot be 100% water [3]. Nevertheless, the presence of porosity has a great repercussion on the shock velocity and the compressibility of the material. As a result, the equations of state differ from the non-porous material. Since all real birds contain cavities and entrapped air, it can be guessed as a first approach that a porous material would produce similar results to the real ones.

The increase in porosity z produces:

- A decrease in shock velocity that provokes a decrease in shock pressure.
- A decrease in density induces a decrease in P_s during the steady flow. However, the compressibility effects, which are enhanced as z increases, oppose that effect producing a very small variation.

To introduce the porosity effect, it is required to add some new modifications to the equations of state shown before (equations (2.1) and (2.2)).

The average density of the material is defined by:

$$\rho_{1B} = z\rho_{air} + (1-z)\rho_{H_2O1} \tag{2.15}$$

The isentropic relationship comes defined by equation (2.16):[2]

$$\frac{\rho_{1B}}{\rho_{2B}} = \frac{\rho_{H_2O1}}{\rho_{H_2O2}} + z\frac{\rho_{air1}}{\rho_{air2}} \tag{2.16}$$

where

$$\frac{\rho_{H_2O1}}{\rho_{H_2O2}} = (P_2/A+1)^{-1/B} \tag{2.17}$$

[2]The subscript 1 alludes to the initial state while the subscript 2 makes reference to the final state.

The material constants correspond to:

$$A = \rho_{H_2O1} c_{H_2O}/(4k_{H_2O} - 1) \qquad B = 4k_{H_2O} - 1 \tag{2.18}$$

And the ratio of densities in air is:

$$\frac{\rho_{air1}}{\rho_{air2}} = (1 - q) \tag{2.19}$$

Finally, establishing q as:

$$q = q_1 - q_2 \tag{2.20}$$

$$q_1 = \frac{2\bar{P}k_{air} + \frac{\rho_{1air}c_{oair}^2}{P_o}}{2\bar{P}k_{air}^2} \qquad q_2 = \frac{((2\bar{P}k_{air} + \frac{\rho_{1air}c_{oair}^2}{P_o})^2 - 4\bar{P}^2k_{air}^2)^{1/2}}{2\bar{P}k_{air}^2} \tag{2.21}$$

Taking in mind that $\bar{P}$ is defined by

$$\bar{P} = P_2/P_1 \tag{2.22}$$

After rearranging equations (2.16), (2.17), (2.19), (2.20) in connection with (2.1) and (2.2), the influence of porosity in Hugoniot pressure is determined. Willbeck estimates that 10% of porosity is the most suitable result in comparison

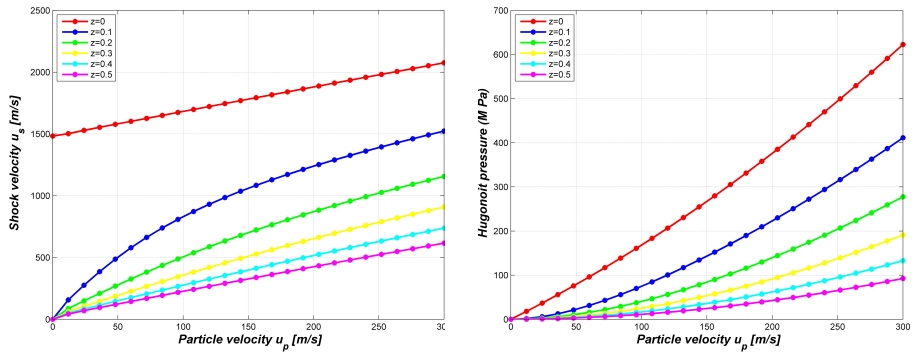

(a) Shock velocity vs. particle velocity (b) Hugoniot Pressure vs. particle velocity

Figure 2.6: Effect of porosity for water

with experimental data.

2.3 Characterization of the bird model

2.3.1 Numerical model for the target

In this section, the target remains the same in every simulation independently of the impactor launched. This structure is modelled as a rigid body to allow focusing on the impactor itself.

Density $[kg/m^3]$	7850
Poisson ratio	0.3
Young modulus[Pa]	$2.1 \cdot 10^{11}$

Table 2.1: Parameters of the rigid plate

The material used is the PAM-CRASH type 100 "Null material for shell elements" and the parameters set in order to simulate the rigid plate are the ones gathered in table 2.1:

Concerning the structure, the shape and dimensions are identical to the ones used for the experimental tests in CRAVHI tests (see figure 2.7). It must be remarked that the mesh is not just a simple quadratic mesh, instead, it has been redefined in the center part where the bird impacts, discretizing it in smaller elements in order to obtain accurate results.

The measurement equipment, the gauges, is replicated with SPH particles in the numerical model, which are placed in every location where pressure gauges were placed in the test. These particles are able to provide information about the pressure in the different locations. They are showed in figure 2.7.

Finally, for the correct simulation, a contact and boundary condition are defined:

- A contact between the impactor and the target is created, this is a contact type 34 in PAM-CRASH notation. This is a non-symmetric node-to-segment contact with edge treatment, i.e. 3D bucket search[3]. For the correct work of the simulation, it is needed to define a master and a slave surfaces. All nodes of the slave will be checked for penetrations due to the segments or edges of the master object.[18]

- The boundary condition located along the whole perimeter of the plate is set to 1 in every direction, i.e. x,y,z and every rotation about the three axis. This means that all degrees of freedom are constrained.

2.3.2 Numerical model for the bird

The detail analysis of the bird is performed in the following section. This is crucial for the study since the whole project is based on the correct characterization of the bird. For this purpose, PAM-CRASH code has been used.

Five steps are followed in the characterization of the bird:

1. The modelling method of the bird is selected. Two different models have been compared and studied: a Lagrangian model and SPH model.

2. Shape analysis is carried out in order to study the influence of the geometry. Three shapes are studied: spherical, cylindrical and a cylinder with hemi-spheres ends.

[3]3D bucket is a research algorithm which divides the surface in a smaller number of buckets (NUMBKT in PAMCRASH's terms) and nodes are recalculated in terms of bucket coordinates.[18]

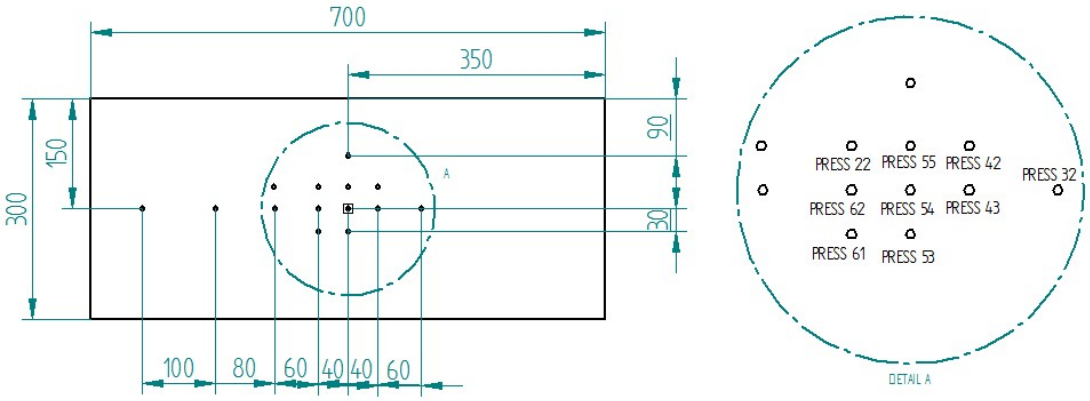

Figure 2.7: Location of pressure gauges (dimensions are mm)

3. Modelization of the bird. Different configurations of particles are created by different methodologies. Besides, some parameters are changed in order to optimize it.

4. Once all the studies are performed and compared with the experimental tests, the suitable model was chosen.

5. Additional sensitivity analyses.

Lagrangian model vs. SPH model

The most appropriate technique of the bird model was not easily undeniable. Taking this into account, alternative approaches have been investigated. In this case, the Lagrangian and SPH model have been put into practise and compared.

Starting with the oldest method in the industry, the Lagrangian bird was implemented. Its dimensions and parameters can be checked in table 2.2.

Properties	**Lagrangian technique**	**SPH technique**
Mass $[lb]$	8	8
Density $[kg/m^3]$	962	962
Particle numbers	5700 (solid elements)	5700 (SPH)
Diameter$[m]$	0.14	0.14
Length$[m]$	0.737	0.737

Table 2.2: Parameters of bird techniques

As it was stated in section 1.4.2, the mesh nodes of the Lagrangian formulation are associated with the particles in the material.

In comparison, the SPH model was put into practice in a parallel way, i.e. using the same parameters, the same target, at the same velocity and location. Similarly, the same information has been gathered in table 2.2. Notice that the density defined takes into consideration 10% of air porosity as Willbeck recommends in both models.

Remembering that the Smooth Particle Hydrodynamics formulation is a gridless Lagrangian technique in which the mesh is replaced by a set of

(a) Lagrangian model (b) SPH model

Figure 2.8: Birds techniques

interacting particles, the previous Lagrangian model was modified: removing the mesh, transforming it into those discrete interacting particles, obtaining the SPH model (see both models in figure 2.8).

In this case, the importance is the definition of the smoothing length (h) of each particle, this is, each particle has a range of interaction with the neighbours which determines the proper performance of the model. To model it, a B-spline option exposed in figure 2.9 is used, being h proportional to the particle's radius, r. The relation h/r is of the order of $1.7 - 2$.

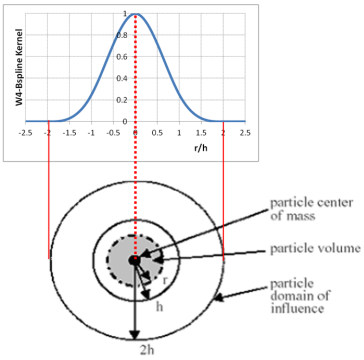

Figure 2.9: B-spline [7]

In the end, the experimental results of CRAVHI project have been used in order to examine the results obtained from FEM simulations at a velocity of 200 m/s.

The most important features are the difficulties in terms of stability presented by the Lagrangian method, as the modelization of fluid like behaviour of these birds, and the distortion of the bird once it has broken up. However, the most significant problem is that the Lagrangian simulation ends prematurely. It is failed because of the excessive compression of elements, which derives into negative volumes. In order to solve it, the solution that was proposed was to put a limit of size from which elements with smaller dimensions are eliminated. The drawback is the increase of CPU time required to perform the operation and in order to reduce such time, the limit was put in the minimum time step. However, all these improvements do not solve the problem and it is still creating a premature failure. A sketch of both simulations is illustrated in figures 2.10 and 2.11.

In addition, because the solution time is proportional to the smallest element size, i.e. the smallest element size gives the time step of the solver; the solution time is longer because the elements are too small.

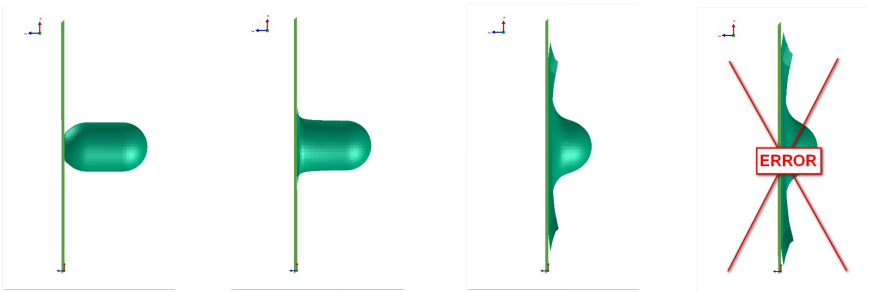

(a) t=0.1 ms (b) t=0.4 ms (c) t=0.8 ms (d) t=1.6 ms

Figure 2.10: Particles displacements of both Lagrangian technique at different times

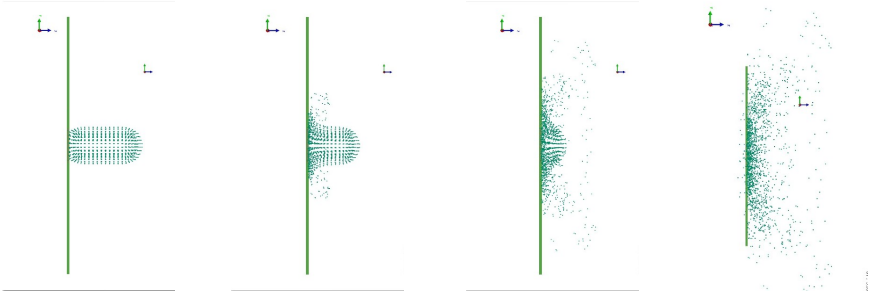

(a) t=0.1 ms (b) t=0.4 ms (c) t=0.8 ms (d) t=1.6 ms

Figure 2.11: Particles displacements of SPH technique at different times

On the opposite side, the SPH model has not had problems concerning simulation failure. Hence, although it requires larger memory space, only the characteristic of non-failure makes this technique suitable. Besides, although Lagrangian bird produces good results before failure, SPH bird fits better the experimental results in terms of pressure and force.

Shape analysis

An important part of the bird strike analysis is the shape of model employed for the simulation. Typical bird shapes are right circular cylinder, hemi-spherical cylinder and sphere.

(a) Sphere (b) Cylinder (c) Hemispherical

Figure 2.12: Shapes of the projectile

For the purpose of this investigation, the three previous shapes depicted in figure 2.12 were considered, all of them keeping the same weight 4 lb (1.8 kg) which is the weight of interest for this research. The characteristics of each model are gathered in table 2.3.

	Sphere	**Cylinder**	**Hemispherical cylinder**
Number of SPH	2134	3630	2484
Density(ρ)$[kg/m^3]$	962	962	962
Length L $[m]$	0.155	0.240	0.202
Diameter D $[m]$	0.155	0.100	0.099
L/D	1	2.4	1.75
Volume$[m^3]$	0.002	0.002	0.002

Table 2.3: Bird shapes parameters

Notice that in each model the same number of particles is maintained, as well as the distance between them. This implies that the total weight is distributed equally among every particle of the projectile.

Moreover, the representation of the pressure is displayed in figure 2.13, comparing with the experimental results from CRAVHI at 200 m/s for a 4 lb bird.[12] This pressure is obtained from the pressure gauge 53 (see figure 2.7). The results from other locations can be found in Appendix C.

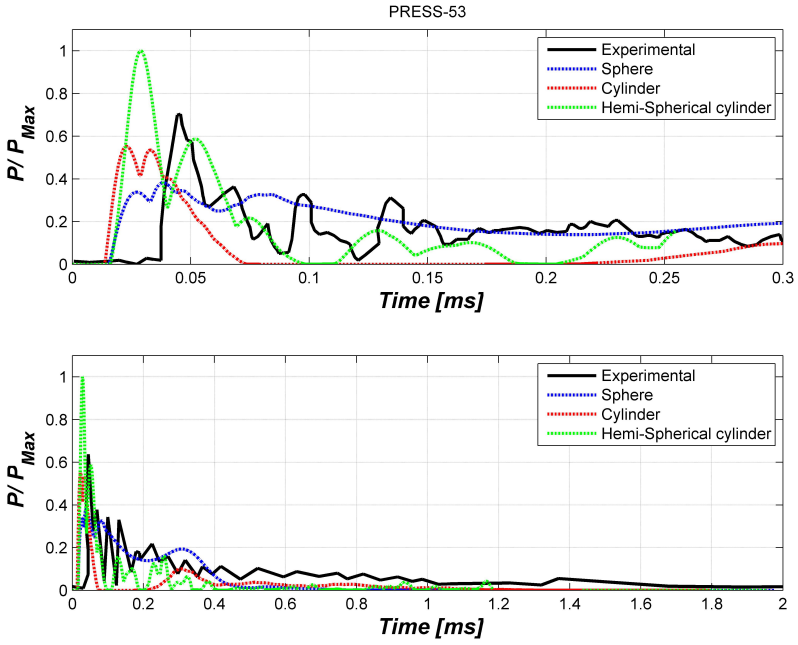

Figure 2.13: Variation of shape

A lot of information can be extracted from the simulation, but the study is focused on the most representative data: the Hugoniot pressure. Moreover, the duration of the impact, the stagnation pressure and the time employed to simulate the results by the program are determinant in order to study the

efficiency of the model. These are the set of factors that characterize the desirability of a possible solution.

Firstly, the duration of the impact is studied. Three comparisons have been performed:

- Numerical simulation vs. Experimental values (Num vs. Exp): the duration of both is compared, taking the initial value in which the bird impacts until the pressure reaches zero value.
- Theoretical value vs Experimental values (Theory vs. Exp): Similarly to the previous analysis, the experimental results are checked with the theoretical value obtained through equation 2.12. This provides an idea of the accuracy of the impact theory.
- Numerical simulation vs. Theoretical value (Num vs. Theo): Finally, a combination of two previous studies is made.

Notice that these calculations give the error obtained from the different analysis with respect to the experimental results.

SHAPE VARIATION: DURATION ANALYSIS

	Num vs Exp	Theory vs Exp	Num vs theo	Total
Sphere	-46,67	-20,77	3,26	-64,18
Cylindrical	-33,33	-48,33	-15,86	-97,52
Hemi-sph	**-23,33**	**-8,67**	**-16,05**	**-48,05**

Figure 2.14: Duration analysis varying shape's bird

It is clear that the sphere spends less time. This is because of its length, which is smaller that the length of the other two cases. Between the other two options, the hemi-spherical cylinder predicts better the time spent in the process. Accordingly, the model with less dissimilarities in terms of duration is the cylinder with hemi-spherical ends, as it is shown in figure 2.14 with a 48% of error, although it is not conservative.

Regarding the pressure analysis, a comparison of the maximum pressure obtained in each pressure gauge with respect to the same values of the experimental data has been computed (see figure 2.15.)

SHAPE VARIATION: PRESSURE ANALYSIS

	HUGONIOT PRESSURE			STAGNATION PRESSURE		
	Sphere	**Cylindrical**	**Hemi-sph**	**Sphere**	**Cylindrical**	**Hemi-sph**
Press 54	-4,67	42,57	132,26	-18,38	-58,65	-51,35
Press 55	-47,22	-0,24	92,04	-12,68	-69,01	-38,03
Press 56	-69,16	23,78	-77,53	-76,16	-37,99	-87,65
Press 53	-33,65	-4,18	73,55	-3,87	-68,5	-83,2
Press 42	-30,18	-18,99	-47,75	6,36	-82,52	-71,67
Press 43	-18,94	-31,79	26,17	-33,09	-70,14	-74,52
Press 32	-98,19	-99,97	-98,37	-100	-100	-98
Press 62	-20,87	-14,16	-45,25	-51,9	-62,57	-67,86
Press 22	-44,2	-33,38	41,038	-41,44	-71,38	-89,67
Press 61	-18,75	-30,46	17,93	-19,4	-47,97	-76,51
Total	**-38,58**	**-16,68**	**11,41**	**-35,06**	**-66,87**	**-73,85**

Figure 2.15: Pressure analysis varying shape's bird

It can be observed in figure 2.13 that the peaks are better adjusted with the hemi-spherical cylinder, and in addition, looking into the other pressure gauges, the peak pressures are not achieved in most of the cases with any of the sphere or cylindrical models. So, in order to be conservative, figure 2.15[4] analysis demonstrates that the hemi-spherical cylindrical model has a better accuracy in the global simulation (11% of positive error, this is, it is conservative).

Besides, a study of the stagnation pressure has been performed, as it can be observed in figure 2.15. For this analysis, the average stagnation pressure has been computed from the numerical and experimental data, obtaining the error with respect to the experimental one. It is shown that the sphere produces a more similar result (-35%), however, as it will be explained later, the cylinder with hemi-spherical ends will be able to improve its stagnation pressure thanks to the variation of viscosity.

Finally, the third study is the CPU computation time. Figure 2.16 shows the different times used for the different shapes.

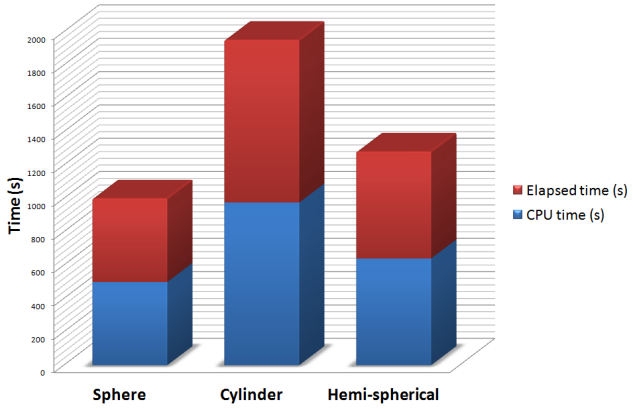

Figure 2.16: CPU time analysis varying shape's bird

It is remarkable the longer time required by the cylinder. Regarding the sphere, it can be said that the reduced duration of the impact is reflected in the CPU time spent.

A final point which is not taken into account in previous analysis is the shape of pressure distribution along time. The pressure from the cylinder with hemi-spherical ends fits better the peaks and the different shapes through time, although the sphere shows a good behaviour as well.

To conclude, the hemi-spherical cylinder predicts pressures being conservative and with consistency over the whole area of impact, not only on the center of impact. Accordingly, this option is taken as the most suitable and it will be taken from now on as the bird shape model for all numerical analysis carried on in this research.

[4]The different gauges located in the tests and in the numerical results correspond to each number as figure 2.7 shows. For example PRESS 54 makes reference to the central pressure gauge.

SPH particles distribution and properties

In this section, the two previous characteristics selected of the model, the cylinder with hemi-spherical ends and the SPH technique, are put into action and a precise study is accomplished in order to improve the final model.

Two different configurations are checked:

- **Configuration A**: It comes from the CRAVHI project [12] in which a transformation from the Lagrangian bird is carried into execution to obtain a SPH model. This bird places the particles symmetrically and radially from the center of symmetry, and the distance between particles, its radius and its volume are not necessarily constant.
- **Configuration B**: This configuration is obtained from a second source which is a Fortran program still under development by *Airbus Defence and Space* company. This code generates a projectile composed of SPH particles in which all particles have the same mass, radius of action, and volume, although the model is not symmetric by definition; the symmetry depends on the inputs that the user enters. Those inputs can be modified by the user, and they are: mass, density and radius of the SPH particle.

Both configurations are shown in Figure 2.17, and the table 2.4 contains the characteristic parameters of both models.

(a) Configuration A

(b) Configuration B

Figure 2.17: Different configurations of SPH particles

	Configuration A	**Configuration B**
Number of SPH	1856	2484
Density(ρ)$[kg/m^3]$	962	962
Diameter D $[m]$	0.100	0.099
L/D	1.737	1.750
Volume$[m^3]$	0.002	0.002

Table 2.4: Configurations A and B parameters

The analysis will consist in the variation of β and α parameters. The parameter α produces a bulk viscosity, while the viscosity associated with β tries to avoid particle interpenetration at high velocities[19]. The suitable range of variation is between 0 and 1.5 for each one. Therefore, both parameters have been varied simultaneously keeping $\alpha = \beta$. However, it has been identified that the effect of β is negligible.

Following the same criteria that in section 2.3.2, an identical analysis in terms of duration, pressure and CPU time has been computed.

Regarding duration of the impact, the increase in viscosity generates a simulation more similar to the experimental results. Comparing both

configurations, results are almost equal: -27.56% and -31.43%. Thus, it seems that the increment of viscosity improves the numerical results.

	VISCOSITY MODIFICATION: DURATION ANALYSIS					
	Source	Viscosity	Num vs Exp	Theory vs Exp	Num vs theo	Total
Viscosity	Configuration A	0	-41	-39,25	-2,88	**-83,13**
		0,5	-40	-39,25	-1,23	**-80,48**
		1	-30	-39,25	15,23	**-54,02**
		1,5	-20	-39,25	31,69	**-27,56**
	Configuration B	0	-37,5	-56,43	23,3	**-70,63**
		0,5	-35	-56,43	25,2	**-66,23**
		1	-25	-56,43	7,12	**-74,31**
		1,5	-15	-56,43	40	**-31,43**

Figure 2.18: Comparison of configurations in terms of duration

Secondly, the CPU time needed to simulate the impacts is increased as viscosity increases. The bird of configuration A shows lower CPU time for all the viscosity range of variation. Thus, configuration A seems convenient until now.

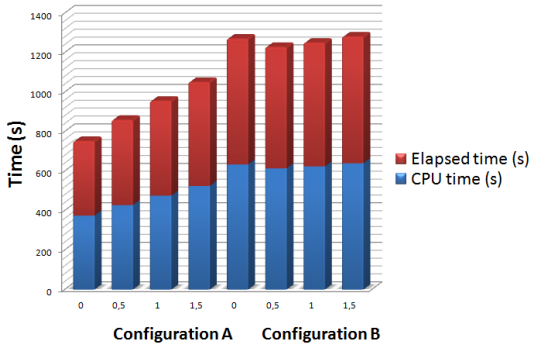

Figure 2.19: CPU time of configurations A and B

Finally, in terms of pressure, it is easily distinguished that the increase of β and α provides similar results compared with the experimental data in both configurations. Pointing out the decrease of peak points of all curves, as the values of β and α values increase.

The percentages presented in figure 2.20 shows that as viscosity increases, the pressure distribution fits better the experimental results, and consequently, the stagnation pressure is closer to the real values.

Moreover, it is interesting to observe the process followed for the birds in the simulation. For the 1.5 value, after the impact, the SPH particles are dispersed in an amorphous way. On the other hand, as the viscosity increases, the particles remain closer, resembling to a real bird strike. This behaviour is appreciated in figures 2.21 and 2.22.

Therefore, it makes sense that the shape of the response is more similar to the real one for β and α equal to 1.5. Therefore, this value is the one selected for the rest of the research. In relation to the selection of one of both configurations, it is important to note the absence of symmetry in configuration B, a feature that provokes that the response obtained is not symmetric. Then, although the

VISCOSITY MODIFICATION

	HUGONIOT PRESSURE ANALYSIS								STAGNATION PRESSURE ANALYSIS							
	Configuration A				Configuration B				Configuration A				Configuration B			
Viscosity	0	0,5	1	1,5	0	0,5	1	1,5	0	0,5	1	1,5	0	0,5	1	1,5
Press 54	137,53	81,16	51,81	34,17	132,27	54,11	15,34	-6,66	-38,59	-79,46	-29,22	-11,35	-51,35	-48,11	-38,38	-18,92
Press 55	5,42	-23,14	-37,22	-38,38	92,04	33,42	14,45	4,42	-29,58	-79,44	-63,8	-12,68	-38,03	-71,55	-63,8	-29,58
Press 56	-69,44	-78,18	-82,86	-86,08	-77,53	-83,88	-89,84	-93,54	-90,72	-86,73	-76,85	-62,55	-87,65	-90,23	-78,4	-70,16
Press 53	5,41	-23,14	-37,22	-38,39	73,55	21,57	-6,12	-9,42	-80,7	-75,92	-68,04	-10,52	-83,2	-78,77	-72,05	10,55
Press 42	-33,32	-51,69	-58,86	-68,36	-47,75	-66,8	-71,21	-62,33	-84,31	-68,18	-78,2	-32,43	-71,67	-57,28	-54,36	-22,76
Press 43	-69,13	-80,03	-85,5	-88,7	26,17	-17,98	-49,2	-66,94	-77,75	-62,21	-47,57	-18,29	-74,52	-62,32	-41,33	-32,51
Press 32	-99,57	-99,99	-99,99	-99,99	-98,37	-99,91	-100	-100	-96	-100	-100	-100	-98	-100	-100	-100
Press 62	-33,28	-51,69	-58,86	-68,36	-45,25	-68,01	-74,46	-70,21	-51,29	-39,95	-29,62	-26,57	-67,86	-45,9	6,19	9,52
Press 22	-70,74	-80,58	-85,38	-88,71	41,04	-10,58	-48,28	-67,62	-68,69	-67,4	-66,3	-56,51	-89,67	-82,98	-69,61	-61,88
Press 61	-69,13	-80,03	-85,5	-88,71	17,93	-25,05	-52,39	-68,39	-53,69	-43,96	-32,21	-1,48	-76,51	-74,97	-33,89	-20,34
Total	**-29,63**	**-48,73**	**-57,96**	**-63,15**	**11,41**	**-26,31**	**-46,17**	**-54,07**	**-67,13**	**-70,33**	**-59,18**	**-33,24**	**-73,85**	**-71,21**	**-54,56**	**-33,61**

Figure 2.20: Pressure analysis for both configurations

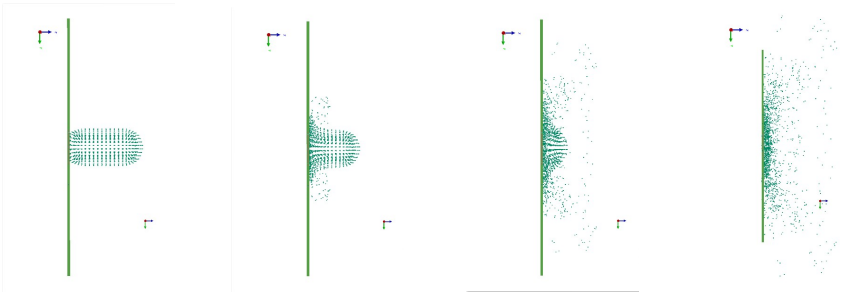

(a) t=0.1 ms (b) t=0.4 ms (c) t=0.8 ms (d) t=1.6 ms

Figure 2.21: Particles displacements of with default viscosity ($\alpha = 0.04$ and $\beta = 0.01$) SPH technique at different times

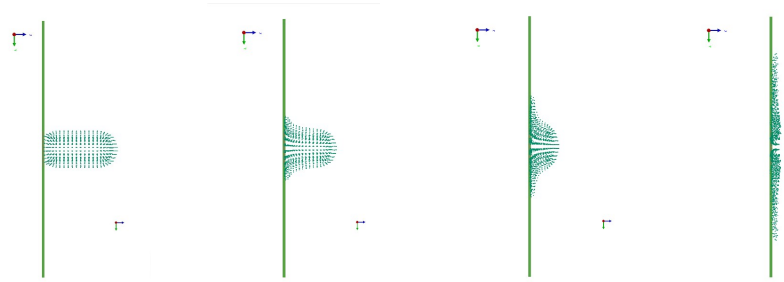

(a) t=0.1 ms (b) t=0.4 ms (c) t=0.8 ms (d) t=1.6 ms

Figure 2.22: Particles displacements with 1.5 viscosity values at different times

data obtained from tests is not symmetric, the simulation should be symmetric, since there are not evidences to simulate in a specific way the anti-symmetries.

Finally, after the whole comparison of both models, the selection of configuration B is concluded. The complete set of characteristics of this model is collected in the table 2.5.

Taking into account that γ and B are required to defined the Murnaghan equation of state needed to describe the SPH bird:

$$P = P_o + B\left(\frac{\rho}{\rho_o}\right)^{\gamma} - 1 \tag{2.23}$$

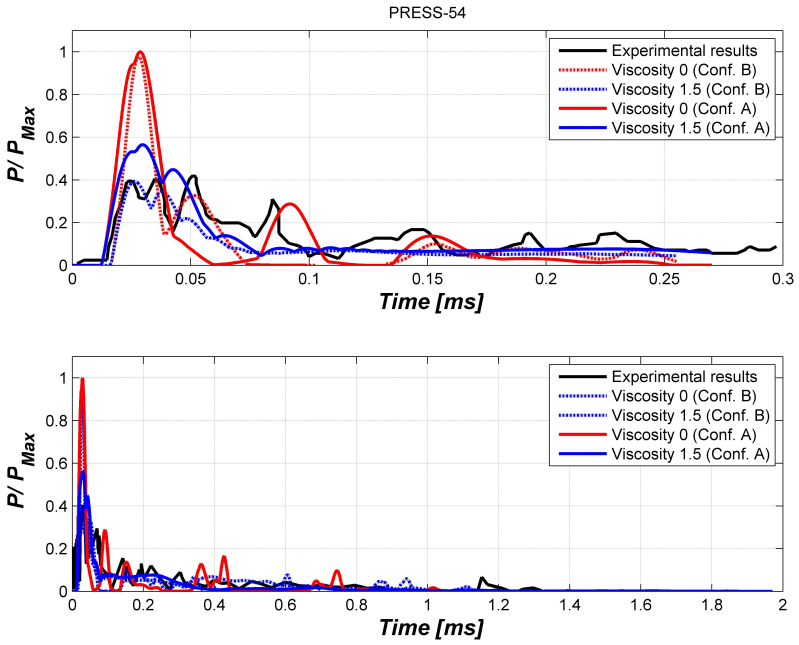

Figure 2.23: Comparison of configurations

Diameter $[m]$	0.1
Length $[m]$	0.21
L/D	1.737
Number of SPH	1856
Volume SPH$[m^3]$	5.73 10^{-3}
Density$(\rho)[kg/m^3]$	962
γ	7.98
Bulk modulus B	128 10^6

Table 2.5: Parameters of bird selected

2.4 Sensitivity studies

To verify the robustness of the solution selected sensitivity studies are done. Several variations in velocity, mass and inclination were performed to understand the performance of the strike.

2.4.1 Speed analysis

The numerical models were created with a 10% of porosity. In order to check the numerical results, an implementation of equations (2.16),(2.17),(2.19), (2.20) together with (2.1) and (2.2) will provide a theoretical estimation of the effect of porosity on pressure as speed is varied.

The presence of porosity has a high effect on the shock velocity and on the compressibility. It can be observed in figure 2.24 how the decrease in shock

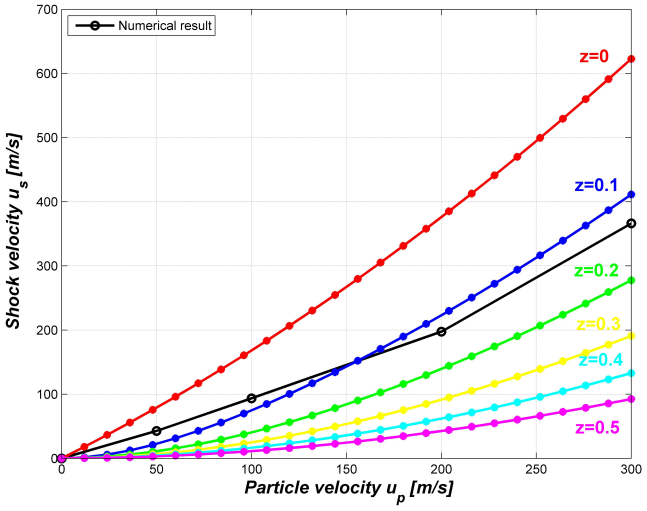

Figure 2.24: Porosity analysis

velocity has as consequence on the decrease of shock pressure.[5]

Therefore, it is concluded that bird simulation and theoretical estimation are very close for porosity z=0.1 (10%).

2.4.2 Energy balance analysis

Basing on the concept of energy conservation, after the impact of the projectile on the target, all kinetic energy is converted to heat and elastic energy due to the deformations and vibrations induced. However, to be able to observe these vibrations and deformations, the impact velocity has not to be very high, since for high velocity there is not enough time to see them. At high speeds, the material behaves in a more brittle way and the forces are applied to fracture the material.

Moreover, energy balances need to be checked for non-liner FEM to check that there are no instabilities. In this analysis, all simulations balance the energy in the appropriated way. This is because the target is rigid and as consequence, no elastic phenomena occurs, which leads to geometric stiffening problems. This stiffening problems are related with exponential growth of internal loads softening the material. Although in such cases the solution becomes stable again, the displacement is larger than the real one.[12]

The theoretical equation which represents the kinetic energy is given by equation 2.24.

$$KE = \frac{1}{2}mV^2 \tag{2.24}$$

The Kinetic Energy is usually used as an indicator of the likelihood of

[5]The properties of the materials (water and air) used for the theoretical representation are: $c_{owater} = 1482.9\ m/s$, $c_{oair} = 342.29\ m/s$, $\rho_{water} = 1000\ kg/m^3$, $\rho_{air} = 1\ kg/m^3$, $k_{water} = 2$ and $k_{air} = 1.03$. These properties fit for $Mach = 1.2$, 1 atmosphere and a temperature of $20^{\circ}C$.

damage from an impact, so its study is a very significant feature. It has been estimated by EASA [20] that 90% of accidents due to bird strikes involve impact energies above 1500 J. Then, it can be observed that a bird flying at 40 m/s almost achieves this energy value, and the same does a bird of 8 lb at 30 m/s. Consequently, it can be seen that both, the mass and the velocity, are determinant factors for bird strikes impacts.

It can be seen in figure 2.24 how the results obtained from the numerical simulation fit very well with the theoretical guess (with a very little error, near 0% for the case of the 4 lb bird).

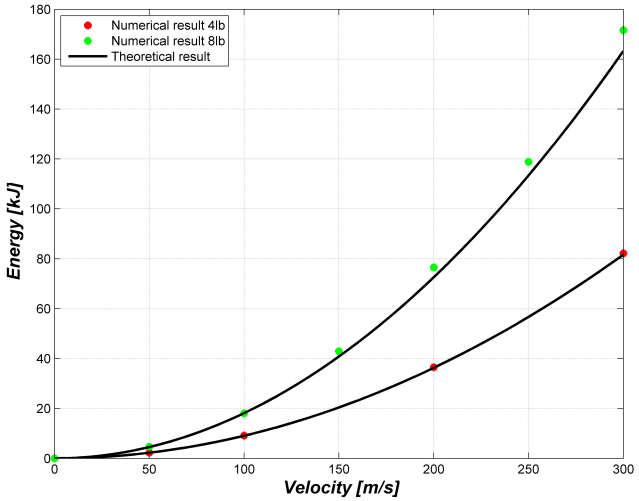

Figure 2.25: Kinetic energy analysis

2.4.3 Mass analysis

In this study, the principal factor has been the mass. It is a very important point, since the regulations focus its requirements depending on the mass of the birds. Three masses have been put into practice: 1 kg, 1.8 kg (4 lb) and 3.6 kg (8 lb), in order to obtain the following results.

Figure 2.26 represents the Hugoniot pressure at a velocity impact of 200 m/s. It is remarkable that the pressure estimated by theory is bigger than the one obtained from PAM-CRASH. However, what is actually important is that mass has not any effect on P_H. Although in the numerical simulation it seems to not be constant, the appearance of some dissimilarities is explained due to the different attributes generated by the codes. In spite of this fact, the tendency is to remain constant as long as the velocity remains the same.

On the other hand, the contact force depends on mass, based on the reasoning of previous equation (2.11). The force in the steady region is proportional to the cross-sectional area of the projectile, the bird. Since the mass of the bird varies but the density remains equal, the volume has to change. Accordingly, the diameter, the length or both of them have to change to fulfil the mass requirement. Then, as mass increases, volume and diameter do the

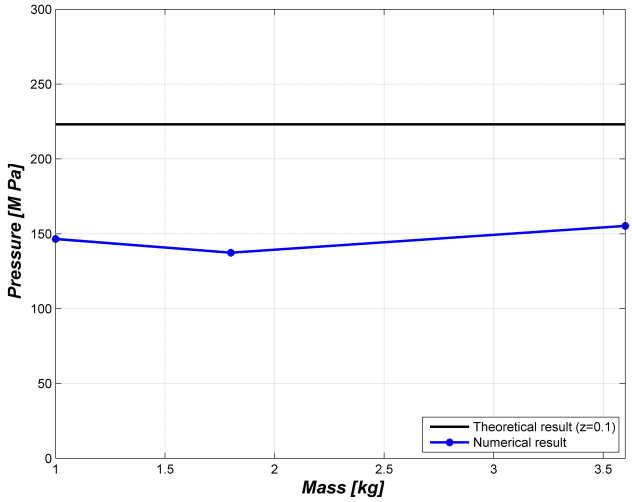

Figure 2.26: Mass variation

same, increasing the force. This makes sense with the results shown previously on Hugoniot pressure(no influence of mass variation on pressure) as pressure is defined as force per unit area. Therefore, although different birds with different weight create different contact forces, due to its dimensions, the area counteracts the differences in force.

The theoretical and numerical forces are illustrated in figure (2.27). Both results are similar. Notice that the theoretical values plotted correspond to the steady flow regime since it is not possible to obtain the theoretical values along the whole impact. The theoretical force corresponds to equation (2.11).

2.4.4 Inclination analysis

This section centers its attention on the investigation of oblique impacts on rigid targets. The difference with previous sections is the direction of the velocity vector, which now is oriented at an angle of the target.

The simulation was performed at 90°, 70°, 45° and 30°, at a velocity of 200 m/s, with the same hemi-spherical model of porosity 10%.

Willbeck predicted through its theory that the Hugoniot shock pressure created in a oblique impact is equal to the one generated by a normal impact with a velocity equal to the normal component of the oblique impact.[12] However, the stagnation point for oblique impact is not equal. This is because this point is not placed at the center of the target, instead, it is moved depending on the angle in the manner of pressure distribution. On the other hand, the value of the stagnation pressure is totally independent on the angle of impact.

Accordingly, figure 2.28 shows that as the bird impacts with a higher angle (understanding by incident angle the angle created between the bird and the target) the pressure generated is higher, in accordance with Willbeck's theory.

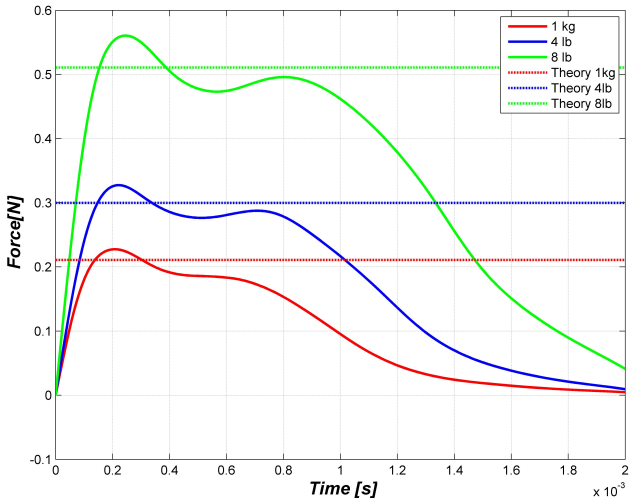

Figure 2.27: Contact force varying mass

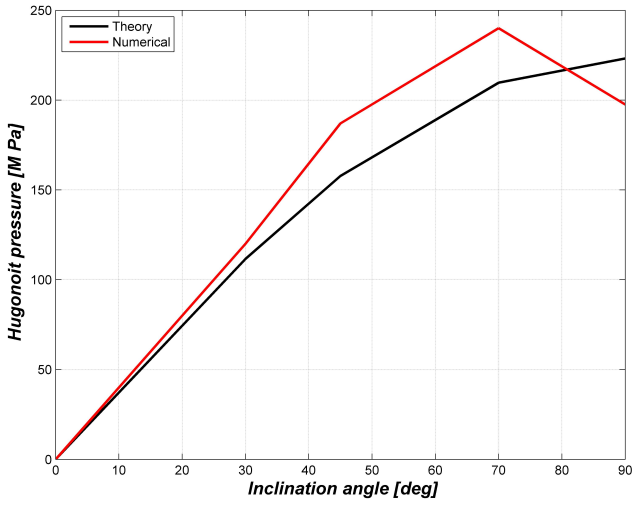

Figure 2.28: Hugoniot Pressure vs. Incident angle

Chapter 3

Flat transparencies

"For every complex problem there is an answer that is clear, simple, and wrong"

- H.L. Mencken, *The Divine Afflatus*

The previous chapter was focused on the investigation of bird impacts on rigid targets, that is without taking into account its flexibility. This was done because the elimination of flexibility oof the target allows the characterization of the bird.

Nevertheless, all real structures have this particular characteristic: they have some flexibility that changes its reaction to impacts. Consequently, flexibility can not be ignored, and it must be studied in order to obtain a more realistic result of the analysis.

The aim of this chapter is to present a detailed analysis of a bird strike in flat transparencies. These flat transparencies are flexible panels which treat to simulate the arrangement and design of windscreens. For this purpose, the chapter will be divided into different sections in which the specifications of the target and its material and structure are explained.

The final bird model selected in section 2.3.2 will be used in the simulations. And Willbeck theory for flexible targets will provide some guidance to check the results obtained from the numerical simulations.

3.1 Transparencies: Aviation Applications

Transparent materials are used in optics field due to its physical property of transparency. This property allows light to pass and have vision through it. The most common transparent material is glass, which has the ability to reflect, refract and transmit light without scattering, which makes it very attractive for transparencies. On the other hand, although it is extremely durable under most conditions, it is brittle, and will tend to fracture.

Transparent materials have a lot of utilities: they can be found in windows, glasses, renewable energy as solar energy glass or wind turbines, radiation protection, insulation, conservatory, packaging (jars, bottles),automotive windshields, etc.

In the aviation field, transparencies can be found in windshields, canopies, or observation bubbles. These structures comprise curved transparent panels fixed to the general structure through frames providing, in addition, structural support. These frames are usually metallic and use fasteners to attach them. Notice the huge discontinuities between material properties of transparencies and frames, making its design very complicated in terms of dynamic loading due to bird impacts. Moreover, in real life, the installation of those kinds of structures generates additional stress and cracks because of fasteners.[21]

Remembering the relevance of bird strike previously exposed, it was reported by EASA [20] that the highest rate of bird strikes belongs to CS-25 aircraft, although the proportion of damage is low (9% of all bird strike accidents); while for CS-27 (helicopters) the damage grows up to 49% of all bird strike accidents, essentially in windshields. Moreover, windshield penetration has occurred in 50% of all accidents, being very critical for safety.

Some examples of those bird strikes are depicted in the following images:

(a) Windshield bird strike
[22]

(b) Harrier Jet bird strike
[23]

Figure 3.1: Examples of bird collisions

In the very beginning, those transparencies were manufactured of glasses due to its transparent properties, however, the low resistance to impacts and its poor properties, as brittleness, made of it a not desirable material for aeronautical applications. So it was necessary the evolution of such transparencies into a material which fulfilled the requirements of transparency but improving the glass properties. Then, acrylic materials were found as an appropriate solution.

Acrylic materials used nowadays, and they are typically Policarbonate (PC)

and Polymethyl methacrylate (PMMA). They have a lot of benefits because of its reduction in weight and good formability, but what is more important is the capability to resist impacts at high velocities.

The design of such transparencies is continuously evolving more and laminated models have been implemented in windshields. This laminated model is composed of several layers in which the interlayer is other type of material.[21]

This interlayer is typically an elastic resin, usually polyvinyl butyral(PVB) or ethylene-vinyl acetate (EVA), which keeps all layers together. Besides it provides more resistance to penetration, reduces weight and deflects 95% of ultraviolet rays from the sun.[24]

For the main aim of this project, the simulation of bird strike on semi-spherical transparencies similar to observation bubbles, it is totally required the correct modelization of the material.

Two parallel analyses have been performed to characterize the materials used in transparencies: a monolithic model composed of one layer and a laminated model composed of three different layers. Both studies were performed since the monolithic case is the one already implemented in the observation bubble of interest and the laminated case is typically used in aircraft windshields.

3.2 Flexible target theory

Real materials are not completely rigid. Materials show certain flexibility during impact as response. Willbeck evolves its theory treating the target as elastic and introducing this characteristic to the equations previously exposed in section 2.2.[3]

At the beginning of the impact, the bird only affects a local area of the target. In this area, the shock wave can be treated as planar and one-dimensional as a first approach, and then the shock equations can be used for both: the target and the bird.

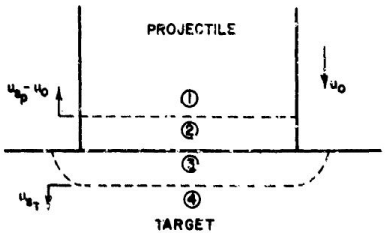

Figure 3.2: Elastic target during early shock wave[3]

Observing figure 3.2, the following equations are obtained:

$$P_2 = \rho_p u_{s_p} u_{P_p} \tag{3.1}$$

$$P_3 = \rho_t u_{s_t} u_{P_t} \tag{3.2}$$

Subscripts 2 and 3 make reference to the shocked region in the projectile and in the target respectively. As equilibrium is needed:

$$P_3 = P_2 \tag{3.3}$$

$$u_3 = u_2 \tag{3.4}$$

Then, the definition of particle velocity is given by equations (3.5) and (3.6)

$$u_{P_p} = u_o - u_2 \tag{3.5}$$

$$u_{P_t} = u_3 - u_4 = u_3 \tag{3.6}$$

Consequently, the particle velocity can be related by:

$$u_{P_t} = u_o - u_{P_p} \tag{3.7}$$

After the whole formulation, rearranging equations: (3.7), (3.2),(3.1) and the equation of Hugoniot pressure, the pressure generated at the interface between the bird and the target is:

$$P = \rho_P u_{s_P} u_o \Big(\frac{\rho_t u_{s_t}}{\rho_P u_{s_P} + \rho_t u_{s_t}} \Big) \tag{3.8}$$

The net result of the target deformation is that velocity between the bird and the target decreases, consequently, the pressure does the same as well. This is due to the reflection of shock waves back to the impact surface, decreasing the shock pressure at that place.[3]

3.3 Flexible target definition

For the numerical simulation of a bird strike on a flat transparency, it is required the same components as in the case of a solid target: a projectile and a target.

The projectile, i.e. the bird, is the model generated in chapter 2: cylinder with hemi-spherical ends composed of SPH with viscosity equal to 1.5, weight of 4 lb (as regulation requires) and porosity z=0.1.

Hence, the aim of this section is the definition of a transparent material as similar as possible to the real one, although the temperature dependency will be excluded of this research.

Then, the characterization of the target was done in several steps:

1. Structure definition: designation of layers and the corresponding contacts and ties.
2. Creation of the mesh
3. Material characterization: integration of properties in order to obtain a real model.

3.3.1 Structure definition

The target is a quadrilateral of 0.7 x 0.7 m and variable thickness depending on the analysis. Two principal elements were defined, contact and links

- **Contacts**:Two different contacts have been used.
  - Contact 34: A contact 34 is applied between the bird and the target.

  - Contact 36: A more detail model is needed for the case of the laminated target, this is why the definition of a contact 36 is needed. The laminated target for this study is composed of three layers; each one with an identical number of shell elements than the simple case (18,940), the monolithic model. Hence, the number of shell elements for this case is three times larger than in the monolithic one (56,820). Due to the presence of these three layers, it is required to add an additional contact between them, a contact type 36. It is a "self contact" that only requires the definition of the slaves surfaces, in this case, the three layers. This checks the penetration due to the other side segments.[18]

- **Links**: It is necessary to define interface links between the layers. These links are called ties and are contacts with a single failure. The slave nodes can be separated from the master surface. The way of working of this interface is through the definition of a box in which all the nodes inside of it will be connected to the master segment. The definition of h_{cont} in the tied interface establishes the link search distance, this is the size of the box. This distance varies depending on the layer's thickness, and consequently two ties for each model must be defined: between upper and middle layers and lower and middle layers.

3.3.2 Mesh definition

Once the structure of the model has been implemented, a deeper study of the mesh was done looking for the star pattern that transparent materials follow after the impact of a projectile, as it is illustrated in figure 3.3.

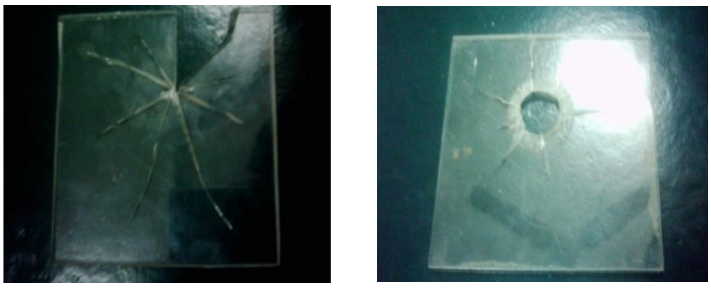

(a) PMMA 4 mm (b) PMMA 6 mm

Figure 3.3: PMMA piece after impact by spherical projectile at v=100 m/s[25]

This star pattern is produced due to the stresses generated in the target. Upon the impact, the area where the bird impacts experiences high stresses in radial and hoop directions. But, the stresses generated in hoop direction are much higher than the allowed tensile stresses; this produces the fracture of the material near the star pattern. Then, as the bird follows its trajectory, the radial cracks appear in the affected zone, creating concentric cracks around the bird. If the velocity is high enough, the bird will progress pushing forward the cracked zone, making a bigger hole than its diameter.[25] This schematic behaviour is shown in figure 3.4.

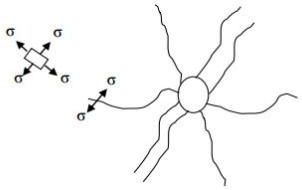

Figure 3.4: Behaviour oh PMMA after impact[25]

Therefore, the correct definition of the mesh is going to help the simulation in order to obtain a similar star pattern once the bird impacts the target. For this purpose, the mesh type has been investigated.

First of all, a structured mesh was created with 3,675 quadrilateral elements. The results obtained were very poor. This was because of the reduced number of elements; therefore, the mesh was refined increasing the number of elements to 117,600 elements per layer. Increasing the number of elements, a more realistic behaviour could be appreciated, however, only perpendicular cracks appeared.

The final solution proposed was the creation of a semi-structured mesh orienting the elements in a circular way, based on the study of TECOSIM [26] for Ford Motor Company. In this study, an impact on a windshield was performed, obtaining the best results with this same type of mesh. For this purpose, TRIA elements were used. The previous process can be observed in figure 3.5.

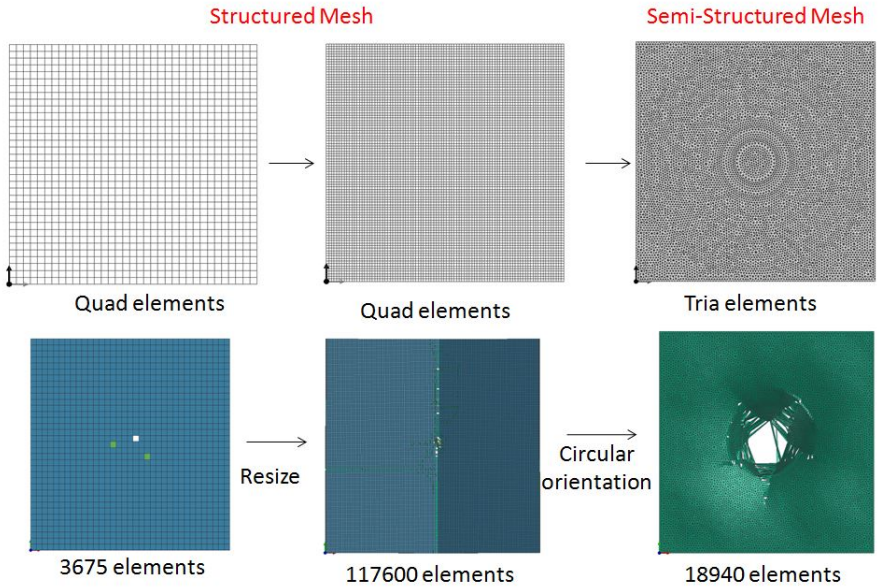

Figure 3.5: Mesh process

The decision to use TRIA elements was taken after several studies. It was observed that this kind of mesh provides the best visual results, producing the star pattern that is known that glass materials produce. But since it has been always recommended to use quadrilateral elements because of its good

properties, it was needed to be sure of the good performance of these elements.

ANSYS GROUP confirms the good behaviour of TRIA elements in ref [27], proving that although in the first years of numerical simulations the finite elements model did not produce good results with this element due to software and hardware limitations, nowadays the current softwares are able to reproduce very good results.

Therefore, following the recommendations of ANSYS, quadratic tria elements have been chosen instead of linear tria ones. Linear elements yield unacceptable approximations in bending moments, since they are too stiff; this is why the mid-side node of the quadratic type provides good results in those cases. Besides, quadratic tria elements are able to produce good results in terms of tension and torsion.

Finally, due to the good visual results and the hints given by ANSYS and because of the lack of experimental data to check it, quadratic TRIA elements were used.

Moreover, the mesh density was increased in the central area where the bird impacted in order to obtain a better accuracy.

Notice that the generation of the circular TRIA mesh was generated with ABAQUS software. Using partitions and defining the number of elements in each partition, the final model with 18,940 elements per layer was obtained and exported to the Visual-Mesh environment.

3.3.3 Characterization of the material

Observation bubbles use monolithic models, while windshields are built of laminated ones. The materials selected for this research are PMMA and PVB. This selection is based on the current aircraft designs: the observation bubble of C-295 aircraft is constructed of PMMA and the front windshields of the same family aircraft, as the C-235, is built of PMMA with an interlayer of PVB.

Thus, a careful characterization of the material is required for further analyses of the observation bubble.

Description of materials

- **PMMA (Polymethyl methacrylate)**

  PMMA is known as Plexiglas, Acrylite Lucite and Perspex. This material is a synthetic, thermoplastic material with derivative of acrylic acid and its properties are its principal advantage: it is tough, transparent (transmits around 92% of visible light in 3 mm material) and has an excellent resistance to ultraviolet radiation and weathering. It can be easily moulded, cut, drilled and formed.

  Moreover, its density varies between 1.17 and 1.20 g/cm^3, which is less than half of the glass density, but what is more important is its good impact strength, although it is lower than polycarbonate's one. Because of this characteristic, its research and implementation has been the objective of military, automotive, aerospace and defence fields.

  On the other hand, its coefficient of thermal expansion is high, meaning that the fractional change in size of the PMMA piece changes as temperature does. And as temperature increases, strain hardening occurs.

Concerning the strain rate, plastic materials have a huge dependence on this characteristic and it is going to be totally determinant for the study. Consequently, the correct characterization of strain rate is crucial for a real simulation.

Figure 3.6 illustrates the influence of strain rates: at low strain rates, PMMA behaves as an elastic material and as strain rate increases, the material becomes brittle. Notice that at high strain rates (of the order of $3400s^{-1}$), the material fails before yielding.[28]

- **PVB (Polyvinil butyral)**

  PVB is a resin used for applications which require strong bonding with high visibility. It is usually manufactured as interlayer for laminated glass because of its properties. This interlayer is able to keep together all layers and prevent from breaking up the material into sharp objects. Although the interest of this model is because of its application on windshields, it is usually applied to sound insulation, objects requiring hurricane-resistant construction or to block ultraviolet radiation.

  The behaviour of PVB can be viscoelastic for long-time behaviour, but elastoplastic or brittle at short time. The failure of this material occurs at high strains, as it is a plastic. Besides, since it is almost an incompressible material, its Poisson's ratio is around 0.5.[29]

  The mechanical behaviour of PVB has been under study because of its importance. Its behaviour for small strains is important to determine bending performance when no cracks appear on the laminated glass. On the other side, large strains are important to understand when cracks appear in laminated glasses, where this material is the link between layers.[30]

  Moreover, it has been observed and proved that it is highly strain rate dependent.

  Figure 3.6 shows that at small strain rates (around 0.2 s^{-1}) the material becomes almost hyperelastic, since non linear deformation occurs until it fails. As strain rates increases, the curves vary and there is an initial gradient that increases as strain rate does.[30]

  In spite of the fact that temperature is other critical factor that has influence over the material properties, it is not taken into account in this project.

Material model

Due to the high dependency on strain rates, the characterization of the model was based on looking for a material type which has the capacity to take into account this characteristic. For that purpose, material type 143 of PAM-CRASH library was applied in a first approach.

Material type 143 (Elastic-Plastic with Elastic Stiffening and Failure for Shell Elements):

This type corresponds to an elastic-plastic model with possibility of stiffening. Its elastic behaviour is determined by the definition of:

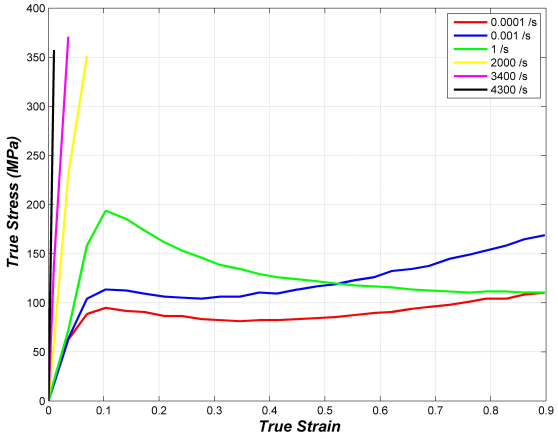

(a) PMMA[28]

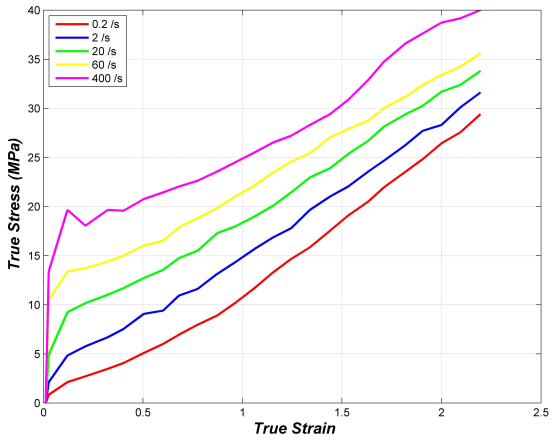

(b) PVB[30]

Figure 3.6: Stress vs. Strain curves at different strain rates

- Elastic modulus (E)
- Poisson's Ratio (ν)
- Thickness

These inputs provide the shear modulus, and at the same time the membrane stiffness, bending stiffness and plate twist stiffness; which relate membrane, twist and bending stresses to in-plane stretch and curvatures.[18]

The strain rate behaviour can be modelled with this material type. This is done through the definition of several curves at each strain rate; then, the software is able of filtering and extrapolate between them to obtain intermediate values, since only eight curves can be defined. However, no yield stress extrapolation beyond the last or first curves is performed, so it is necessary

to be sure that the simulation is in the range of strain ranges that are defined. [18]

Regarding element elimination, because of lack of material properties, it was not possible to use material types whose failure criteria is based on Johnson Cook Model, for example. But the type 143 offers the opportunity to define the maximum total strain as a function of strain rate using a curve. This curve is the definition of critical strain against the logarithm of the strain rate. [18]

Once all the properties were defined, the results obtained were not trustful. Huge deformations were produced without failure at high speeds, and the star pattern was not displayed. And it was needed velocities of the order of 500 m/s to found some cracks or broken elements. Searching in literature and in some researches, it was found that failure velocities for these plastic materials are smaller, and although it presents huge deformation, the failure of the material is achieved before.[25]

Consequently, a revision of the model was done to find the problem. The problem appears with the definition of the stress vs. strain curve at different strain rates. PAM-CRASH needs to input the different curves with the same number of points in abscissa axis. However, at high strain rates, the material fails at lower strain and these curves have less number of points. It was decided to define the same number of points in all curves, and the high strain rate ones will keep constant the failure value of stress along all strains values from that point. This definition should work since the critical strain curve provides the corresponding critical failure strain as a function of strain rate.

It is checked in figure 3.7 how PAMCRASH is not extrapolating in the desired way because the numerical results obtained can belong to strain rates between 1 s^{-1} and 1000 s^{-1}, although it does not follow the strain rate failure criteria.

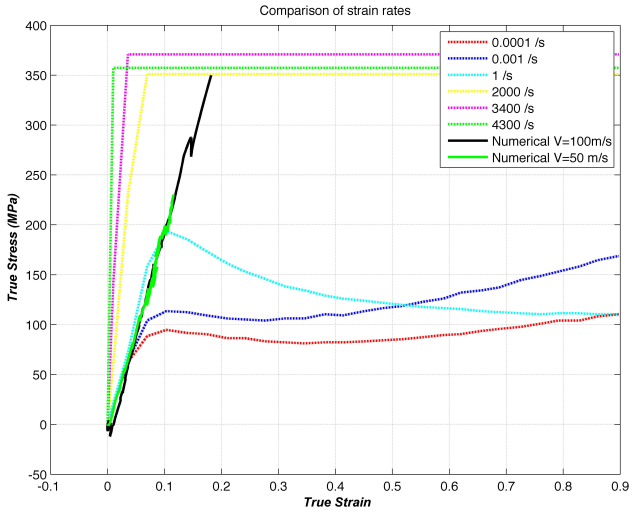

Figure 3.7: Strain rates: numerical behaviour using Material type 143

Consequently, the results were not trustful and it was decided to change the material type.

As it was already said, there is a lack of material properties, and it is pretty

difficult to find the properties of these materials for high strain rates. Then, the material type 126 was implemented.

Material type 126 (Glass Model):

This model describes a linear elastic material with failure criteria.

The fracture criterion is based on Rankine Criterion: the fracture begins when the maximum principal stress on the top or bottom surfaces reaches the critical value, and there is not failure when all stresses are compressive. In addition to this, the crack propagation is defined by an orthotropic damage tensor.[18]

Moreover, the material damping is set to 0.05 and the stress filtering is 10 microseconds to avoid the influence of transient vibration.[18]

In a first approach, it looks perfect for the definition of glasses, as it is recommended by PAMCRASH for the simulation of windshields with an interlayer of PVB. However, for the case of this research, this material type does not have the possibility to define the properties as a function of strain rates.

Therefore, the properties implemented on this model are based on engineering criteria and they are gathered in table 3.1. These values are obtained between strain rates 1 s^{-1} and 1000 s^{-1} in which due to typical bird velocities strain rates for these kind of impacts occurs.

	PMMA	**PVB**
Young's Modulus (E)[GPa]	3.25	9.17
Critical Failure Stress(σ_{cr})[MPa]	300	310
Density(ρ)[kg/m^3]	1190	1100

Table 3.1: Material type 126: material properties

Next section demonstrates that this model reproduces realistic results and in addition it is able to obtain the star cracks pattern.

3.4 Numerical results and discussion

After the complete definition of the way of modelling the transparencies, the two cases have been implemented:

- The monolithic case composed of only one layer of the previously exposed PMMA
- The laminated model composed of three layers; the outer and inner ones correspond to PMMA material while the interlayer is made of PVB.

For those cases several simulations have been performed varying velocity and thickness, and the results have been analysed and compared as follows.

3.4.1 Thickness variation

The variation of thickness is an important factor to be investigated due to the relation with weight. Engineers always try to reduce as much as possible the

weight of aircraft since it is extremely important for operating in a safe and efficient way.

Consequently, it is desired to have the minimum weight for every structure, including observation bubbles but fulfilling the requirements imposed.

Since there is not experimental data for this test, the only way to validate it is through the application of theory aforementioned in section 3.2.

Notice that this previous theory does not have into account the possibility of having a laminated material. Nevertheless, as in this research both solutions are investigated, it is required to deal with this model as well.

For that purpose, in a first approach, it has been calculated an equivalent monolithic plate. In that manner, an equivalent modulus E_e and equivalent density can be identified with the same flexural and axial stiffness as it is illustrated in figure 3.8. The process that has been followed is [31]:

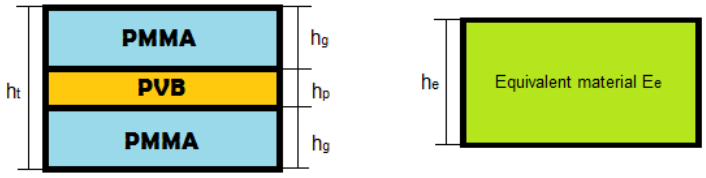

Figure 3.8: Makeup of two-ply laminated glass and an equivalent monolithic material

1. Calculation of the flexural stiffness per unit breadth can be expressed as:

$$FS = F_1 EI = F_2 E_g \frac{h_t^3}{12} = E_e \frac{h_e^3}{12} \tag{3.9}$$

   Being EI the stiffness of the whole laminate plate, and F_1 a reduction factor which allows the reduction of shear deformation of PVB which at temperature of 20°, it is typically 1. The factor F_2 with F_1 reproduces the effect of lower stiffness of the fully composite section of the same total thickness.

   The subscript 'g' stands for the properties of PMMA while the subscript 'p' for PVB.

2. The axial stiffness per unit breadth of the laminate plate is defined as:

$$AS = \sum AE = E_g \sum h_g + E_p h_p = F_3 E_g \sum h_g = E_e h_e \tag{3.10}$$

   F_3 is a factor to take into account the contribution of PVB to tensile stiffness, although this increment is small.

3. Combining equations (3.9) and (3.10), the equivalent material thickness is obtained:

$$h_e \cong \sqrt{\frac{F_1 h_t}{\sum h_g}} E_g \tag{3.11}$$

4. Substituting equation (3.11) into (3.10), the equivalent Young's modulus is obtained:

$$E_e \cong \sqrt{\frac{\sum h_g^3}{F_1 h_t^3}} E_g \tag{3.12}$$

5. Finally, the equivalent density is given by equation (3.13):

$$\rho_e = \frac{m_g}{V_t} + \frac{m_p}{V_t} \tag{3.13}$$

The equivalent density and Young's modulus are used in equation (3.8). And the comparison with numerical results is illustrated in figure 3.9

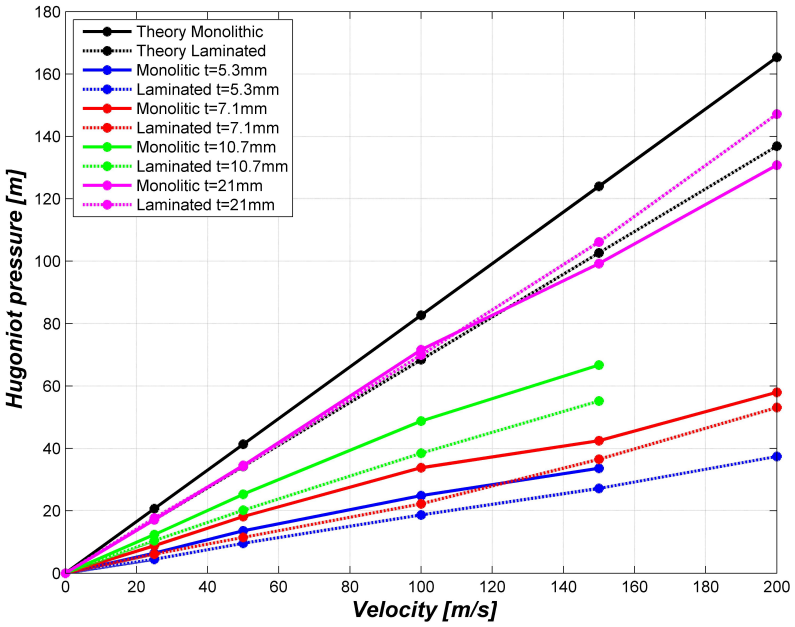

Figure 3.9: Maximum pressure vs. velocity

In this analysis, four different models have been used, from 5 mm (typical thickness of observation bubbles) to 21 mm (typical thickness of whindshields). The different configurations can be checked in table 3.2

Thickness[mm]	Monolithic Model (PMMA)	Laminated model(PMMA-PVB-PMMA)
5.35	5.35	2.5-0.35-2.5
7.13	7.13	3.33-0.47-3.33
10.7	10.7	5.0-0.7-5.0
21.4	21.4	10.0-1.4-10.0

Table 3.2: Thickness and mass properties

From figure 3.9 it is clearly identified how as thickness increases, the theoretical values are more accurate than for smaller thickness. This tendency

is valid since Wilbeck's theory treats the target as a flexible material, i.e. it is an elastic material without permanent deformation or rupture. When the thickness increases, the material starts to behave elastically since the thickness is too big that the projectile, this is the bird, is not able to break it down. For thin targets, the bird deforms and breaks the material; consequently, it does not behave as an elastic target.

Notice that a unique theoretical value is obtained, this is due to the consistency between the shock velocity and density independently of the thickness which are defined by equations (3.14) and (3.15):

$$u_{s_t} = \sqrt{E_e/\rho_e} \tag{3.14}$$

$$\rho_t = \rho_e \tag{3.15}$$

Comparing both models, monolithic and laminated cases, it is evident that at a same impact velocity, laminated model is subjected to a smaller pressure. This is due to the interlayer effect, which gives strength and flexibility to the model.

3.4.2 Ballistic limit

In this section, the penetration and behaviour of the model after the impact is studied using a ballistic limit. This ballistic limit provides an estimation of the critical velocity at which the bird is going to break the transparency.

It was observed and checked that upon the impact, the stresses generated were larger in the impact zone creating the aforementioned star pattern. Moreover, once the velocity is high enough to break the target completely, the impact velocity is very close to the residual velocity, meaning that the target is not able to stop the bird (this is the reason of the linear relationship at high speeds showed in figure 3.10.)

Similarly, due to the lack of experimental data, the results cannot be validated. However, the results are in concordance with similar analogous experiments exposed in paper [25]. And moreover, knowing that the laminated model with 21 mm of thickness simulated in this analysis is very similar to the real windshield of C-235 aircraft and that this structure has fulfilled the requirements imposed by Airworthiness; it can be checked that for its cruise velocity (248 kts, 125 m/s) the model is able to withstand the impact of a 4 lb bird without failure, since the ballistic limit is estimated around more than 140 m/s.

Notice the difference between ballistic limit for a thickness of 5 mm, which is around 100 m/s, while for thickness of 21 mm is near 140 m/s, and even more for laminated models.

Therefore, as thickness increases, the resistance of the material is bigger, and consequently, the bird velocity required to break the transparency is higher. This is because an increment in thickness produces a higher absorption energy, leading to a more resistant material to impacts.

As a final point, some examples of collapse sequences are depicted in the following figures. At 50 m/s, the target does not fail and the elastic properties are showed, while at 150 m/s, the material has already failed and the bird has

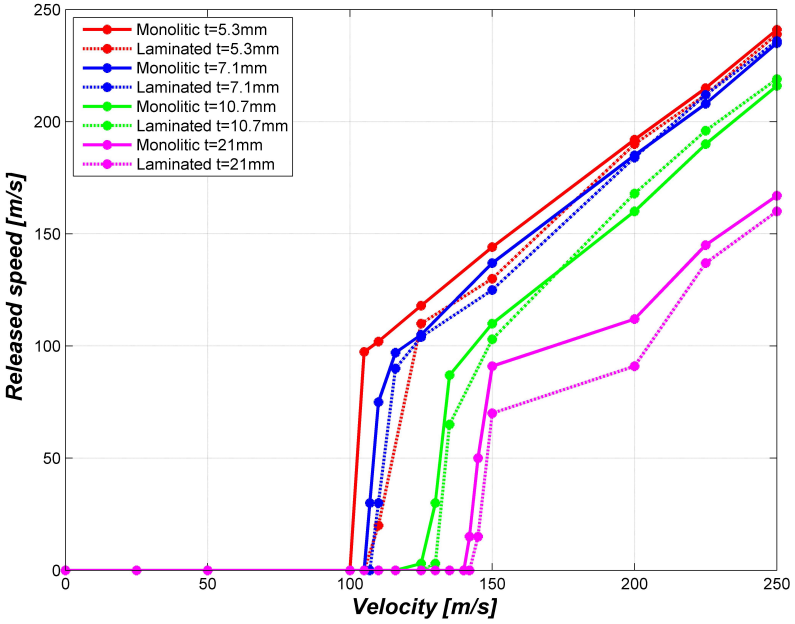

Figure 3.10: Ballistic limit of flat transparencies

enough speed to pass the target. In that last case, the material shows cracks and no elastic properties.

In the case of 50 m/s, the kinetic energy of the bird is transformed into elastic and vibrations due to deformations plus the residual velocity of the bird particles. But at high velocity, there is not enough time to deform and vibrate, and the material behaves as a brittle one in which all energy is employed to break and fracture the material.

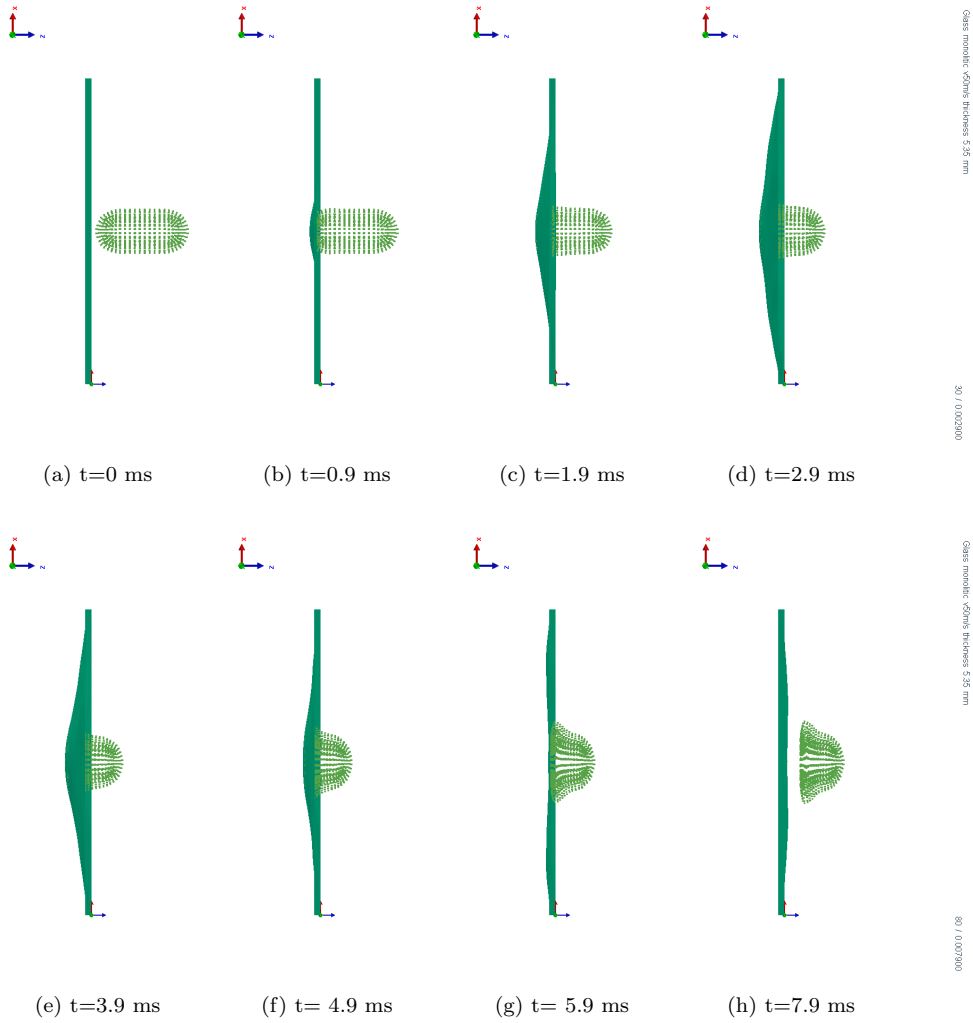

(a) t=0 ms (b) t=0.9 ms (c) t=1.9 ms (d) t=2.9 ms

(e) t=3.9 ms (f) t= 4.9 ms (g) t= 5.9 ms (h) t=7.9 ms

Figure 3.11: Collapse sequence for monolithic case (t=5 mm) at 50 m/s

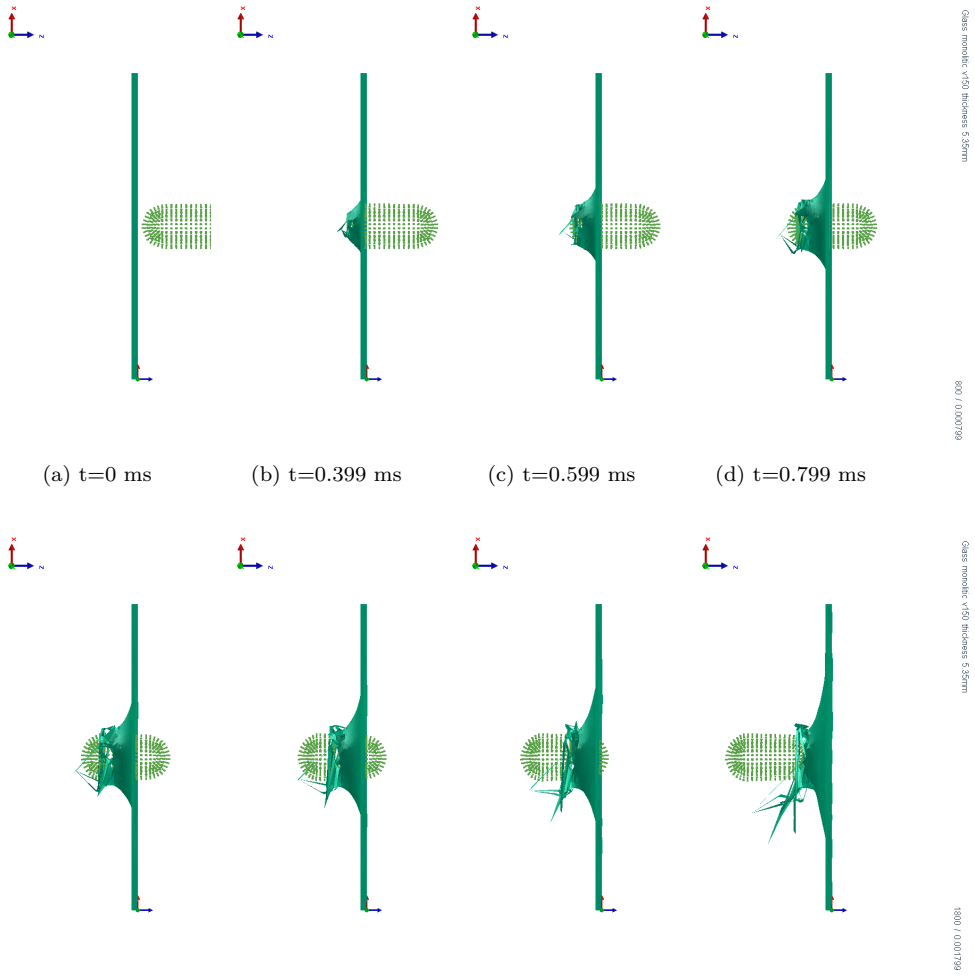

(a) t=0 ms (b) t=0.399 ms (c) t=0.599 ms (d) t=0.799 ms

(e) t=0.999 ms (f) t= 1.199 ms (g) t= 1.399 ms (h) t=1.799 ms

Figure 3.12: Collapse sequence for monolithic case at (t=5 mm) 150 m/s

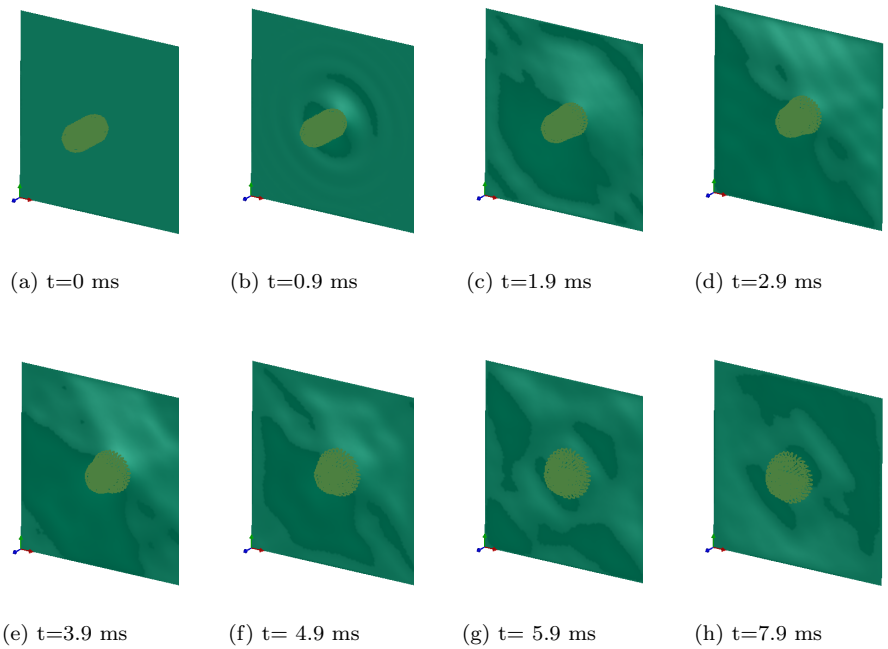

(a) t=0 ms (b) t=0.9 ms (c) t=1.9 ms (d) t=2.9 ms

(e) t=3.9 ms (f) t= 4.9 ms (g) t= 5.9 ms (h) t=7.9 ms

Figure 3.13: Collapse sequence for monolithic case (t=5 mm) at 50 m/s (Isometric view)

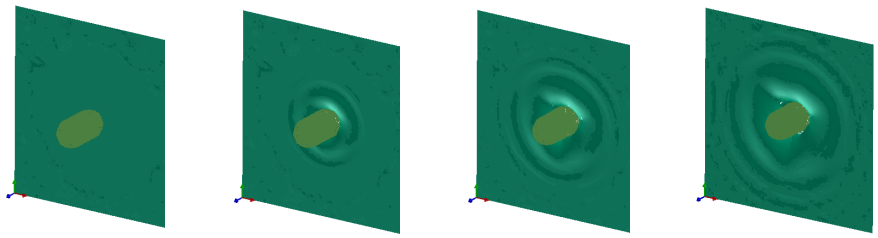

(a) t=0 ms (b) t=0.399 ms (c) t=0.599 ms (d) t=0.799 ms

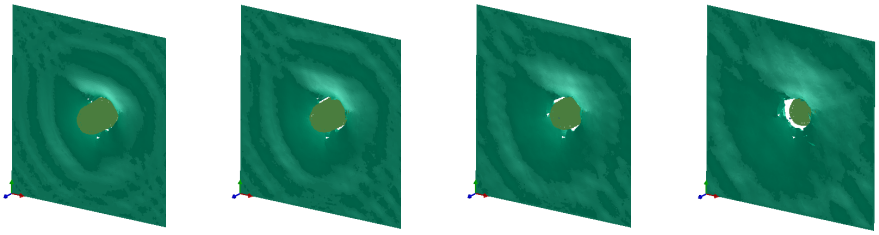

(e) t=0.999 ms (f) t= 1.199 ms (g) t= 1.399 ms (h) t=1.799 ms

Figure 3.14: Collapse sequence for monolithic case (t=5 mm)at 150 m/s(Isometric view)

Chapter 4

Semi-spherical transparencies

"Real knowledge is to know the extent of one's ignorance"

- Confucius,

4.1 Introduction

The last major objective was the simulation of the bird strike in a semi-sphere in order to obtain a first approach of the consequences that a bird strike will produce in the observation bubble of the C-295 aircraft.

After the previous stages described in the two previous chapters were defined, and after characterizing the designation of the bird and the transparency models, the semi-spherical shape was integrated in a FEM.

Figure 4.1: Observation bubble.C-295 Persuader[6]

The present chapter contains several numerical investigations, which have been carried out in terms of thickness of the target, speed or even position of the bird. These factors are critical features for the behaviour of the bubble and will be determinant for the definition of the limit case to ensure safety.

4.2 C-295 aircraft: Spotter Bubble Window

The Airbus Defence and Space C-295 is a developed version of the well-known CN235 aircraft with greater capacity and range. This aircraft is a medium-weight vehicle; very robust, reliable and highly versatile, but what is remarkable is its excellent manoeuvrability, low fuel consumption and long endurance (11 hours).[6]

Due to its strong landing gear, C-295 is able to land and take-off in the more difficult areas and at the same time in a short performance. This aircraft can do any type of mission from personnel, troop and bulky cargo transportation to evacuation, communication duties, search and rescue, surveillance and control, homeland security or certified air-dropping.[6]

For missions of search and rescue, and surveillance and control as the C-295 Persuader, aircraft include bubble windows. These bubble spotter windows facilitate surveillance, search and rescue activities thanks to the wide field of vision. These observation areas are located at both sides of the fuselage at front and aft of the aircraft, making a total of four bubble spotter windows. They are able to provide optimal conditions for visual research and a full panoramic coverage beneath the aircraft. Inside, the C-295 is equipped with spotter's seats to ensure full search coverage, and these bubbles have the option to be opened at low speed and altitudes[32]. They can be observed in figure 4.2.

(a) Spotter bubble window (b) Seat's spotter configuration

Figure 4.2: Configuration of C-295 aircraft[32]

4.3 FEM definition of the bubble

This section deals with the geometrical description of the bubble, the boundary conditions imposed in the FEM and the description of the mesh.

The bird and material elements integrated in this simulations are the ones defined in sections 2.3.2 and 3.3.3 respectively, this is a SPH model of 4 lb bird and a material type 126 with PMMA properties gathered in table 3.1.

4.3.1 Structure of the bubble

The selected shape is not exactly the one of the real observation bubble, but it is defined in that way for the sake of simplification and to take a conservative approach. Taking into account that the bubble has variable thickness, a minimum thickness is implemented in the model, more specifically of the order of

5.3 mm. Similarly, although the bubble is not semi-spherical, the FEM modelled as a semi-sphere with a radius 0.25 m provides conservative results in comparison with the real observation bubble.

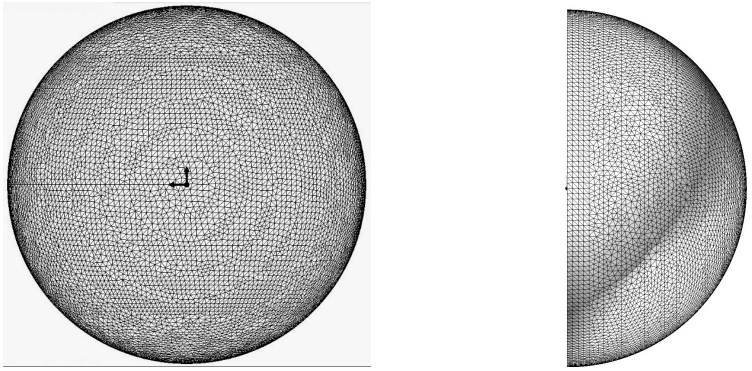

(a) Top view (b) Side view

Figure 4.3: Observer Window FEM

Figure 4.3 shows the FEM model implemented in PAM-CRASH software. Concerning the real distribution of thickness and dimensions of the bubble, since this data is confidential, real numbers cannot be provided.

4.3.2 Boundary conditions and mesh definition

Regarding the boundary condition, the six degrees of freedom have been restricted in the line of support, i.e. displacements and rotations, in order to simulate the fuselage's assembly.

Finally, the mesh used is composed of 14,402 shell elements, based on the same model than for the transparencies cases. Similarly, the mesh has been designed in such a way that tries to reproduce the same star cracking pattern than the real glasses. Then, creating circular patterns to guide the cracking and failure behaviour once the bird impacts its target, the observation bubble is fully defined. And it can be checked in figure 4.4 that the star pattern also appears.

4.4 Semi-spherical transparency simulation

After the whole definition of the semi-spherical model, several simulations were launched to the end of understanding the behaviour and checking if the configuration is able to fulfil the requirements imposed by authorities.

The study is divided into several stages: first of all, a variation of the bird location impact is carried out, which is interesting since the structure is damaged and fails in different ways. Secondly,a study has been performed in order to comprehend the influence of curvature. And finally, variation of the thickness and concluding remarks in terms of fulfilment requirements.

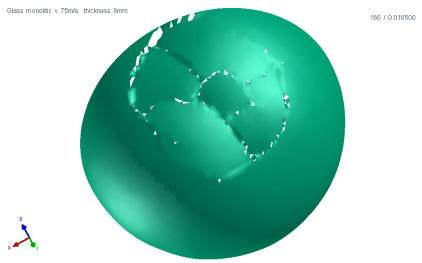

Figure 4.4: Observer Window FEM star pattern (t=8 mm at V=75 m/s)

To deal with all previous stages, the ballistic limit is the method used which provides the maximum speed at which the the bird is not going to penetrate or break the window.

4.4.1 Impact location variation

The impact location of the bird can be critical to understand the behaviour of the bubble under those strikes. For that purposes, several positions have been simulated, from a position too close to the fuselage, the boundary condition, to a position near the tip of the bubble. The pictures of figure 4.5 show the two extreme conditions.

(a) "Position 1" (b) "Position 2"

Figure 4.5: FEM bubble: Position's variation

Speed has been varied for both positions to obtain the ballistic limit. Interesting results have been obtained: the "Position 1" is more critical in terms of ballistic limit: the limit speed is lower and it increases as the bird goes away to the fuselage. The numerical value obtained is about 50 m/s for "Position 1" while the "Position 2" improves the ballistic limit around 20 m/s, this means that the limit speed equals to 70 m/s. The characteristic ballistic limit coming from the numerical simulations is plotted in figure 4.6.

However, as the bird moves away from the boundary condition, the failure area is much bigger, although it requires a higher velocity to run through the bubble. And consequently, when the bird goes through the bubble, the hole is smaller in "Position 1" than the hole created due to the bird strike in "Position 2".

It is important to remark that the position near the fuselage can not be simulated too close to the boundary condition, since simulation errors appear, providing wrong results.

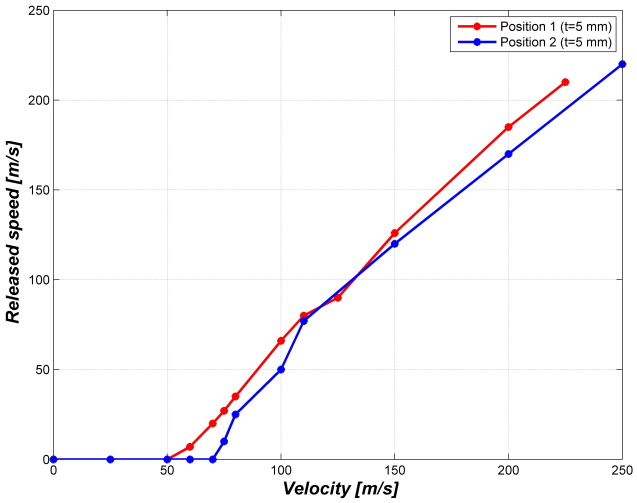

Figure 4.6: Position's variation:Ballistic limit

4.4.2 Influence of curvature

The effect of curvature in transparency is also investigated. Since the principal characteristic and difference between flat transparencies and semi-spherical transparency is its geometry, this is the curvature, a clear understanding of what are the effects of this change is needed.

For that purpose, the ballistic limit was obtained for both configurations: a flat transparency and a semi-spherical one of 5.3 mm of thickness. Note that in order to make possible the comparison, the impact on the semi-spherical shape must be performed in the center of the sphere, simulating a bird strike perpendicular to the fuselage, to avoid the in the boundary condition. These results are illustrated in figure 4.7.

It is remarkable that the semi-spherical shape has a much lower limit velocity, it fails at 50 m/s, while the flat transparency is able to withstand until 105 m/s. However, it can be appreciated how the semi-spherical shape is able to better stop the bird, since the released speed is lower at the first stages. On the other hand, after failure, the flat transparency reduces less the bird speed, obtaining almost a linear relation between velocities ($V_{Released}$=$V_{initial}$).

Then, to understand why this difference occurs, the stress diagrams of both cases were studied. It was found that the curved transparency experiences

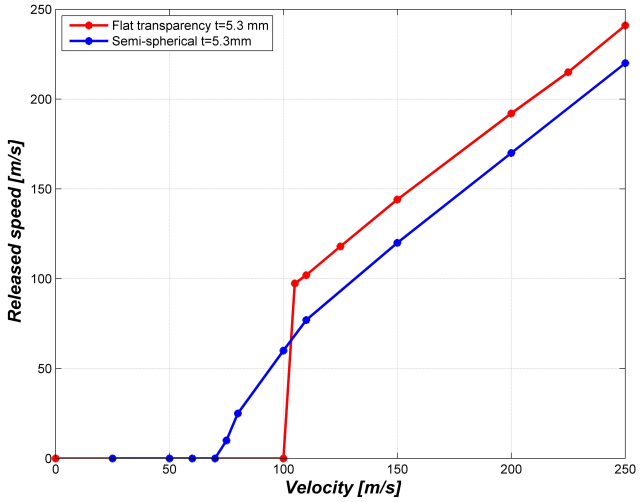

Figure 4.7: Ballistic limit comparison between flat and semi-spherical transparencies

higher effective stresses in magnitude than flat transparencies at the beginning of the strike. This is because of the higher stiffness of curved transparencies.

4.4.3 Thickness variation: Ballistic limit

A study of the thickness influence was performed, similarly to the one studied for flat transparencies. Similar behaviour is observed: as thickness increases, the resistance to impact is higher, allowing higher speeds before failure.

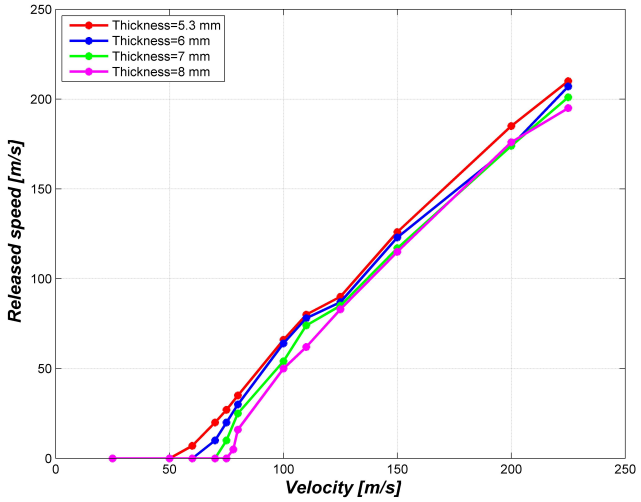

Figure 4.8: Ballistic limit: variation of thickness

Notice that as it was previously stated, the bubble is able to stop the bird to a greater extent, moreover, it can be observed that the slope of the ballistic limit is greater for smaller thickness. This agrees with previous ideas, since as thickness increases, the transparency is able to stop partially the bird.

Nevertheless, for the current model of 5.3 mm of thickness, the limit speed is around 50 m/s. This means that it is too far way of the regulation requirements imposed for this kind of structures, more specifically for this type of aircraft. It was mentioned that the structure must be able to withstand a 4 lb bird impact at sea level and V_c conditions. For this aircraft V_c is 260 kts, this is 133.33 m/s. Obviously, the actual preliminary results obtained for 5 mm thickness does not fulfil this requirement.

Following figures show the different phases of the collapse at two different speed. It can be easily observed as for low velocity below the ballistic limit, this is 25 m/s, the structure is able to withstand the impact without failure. On the opposite side, at higher speed than the ballistic limit i.e. 150 m/s, the bubble fails completely.

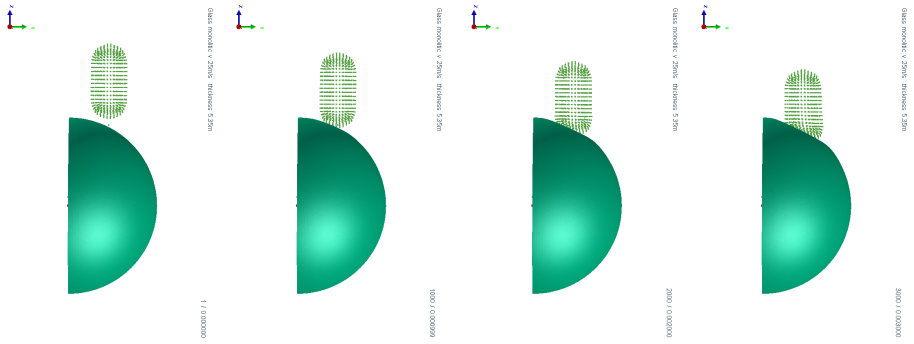

(a) t= 0 ms (b) t= 0.99 ms (c) t= 2 ms (d) t= 3 ms

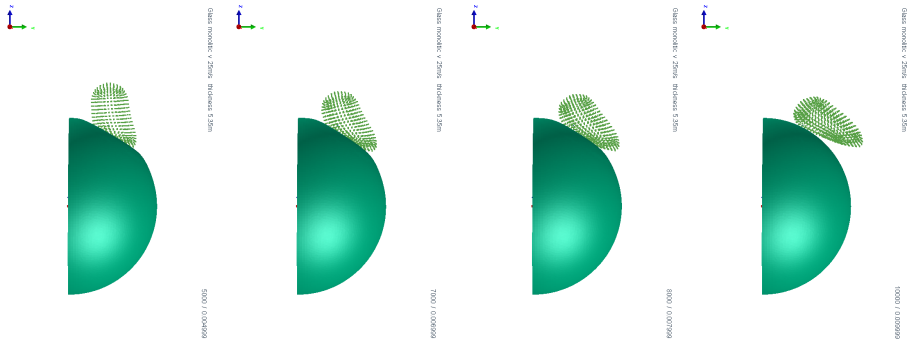

(e) t= 5 ms (f) t= 6 ms (g) t= 7 ms (h) t=10 ms

Figure 4.9: Collapse sequence for monolithic bubble (t=5 mm) at 25 m/s

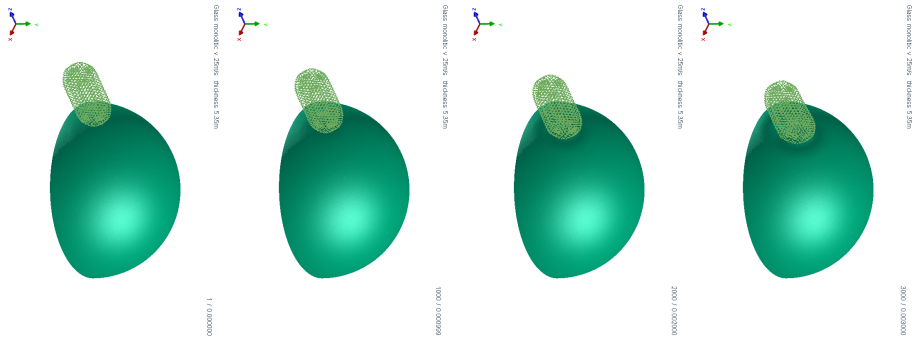

(a) t= 0 ms (b) t= 0.99 ms (c) t= 2 ms (d) t= 3 ms

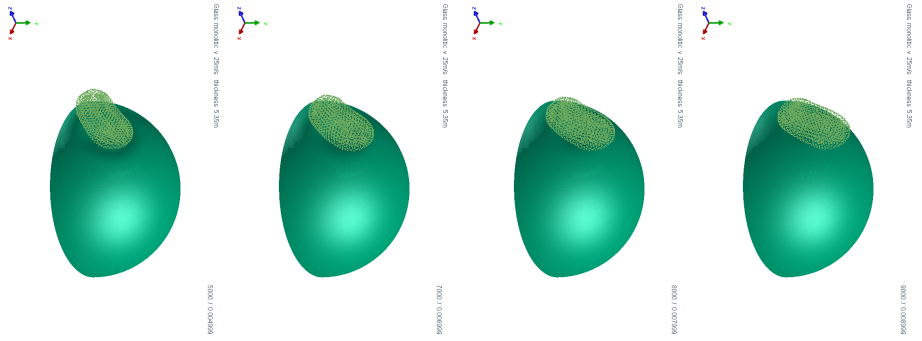

(e) t= 5 ms (f) t= 6 ms (g) t= 7 ms (h) t=9 ms

Figure 4.10: Collapse sequence for monolithic bubble (t=5 mm) at 25 m/s (Isometric view)

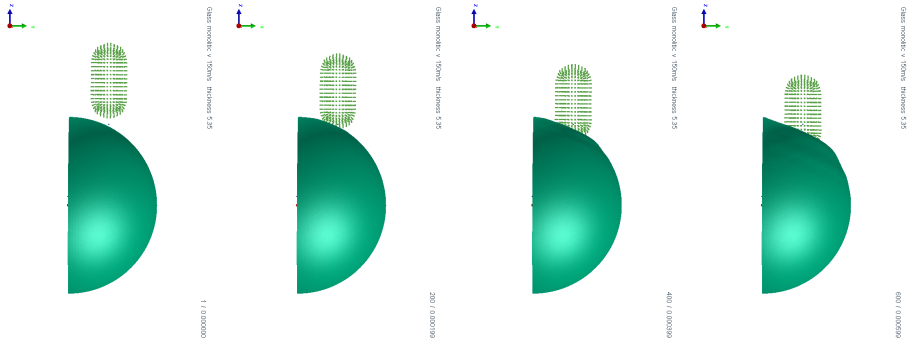

(a) t= 0 ms (b) t= 2 ms (c) t= 4 ms (d) t= 6 ms

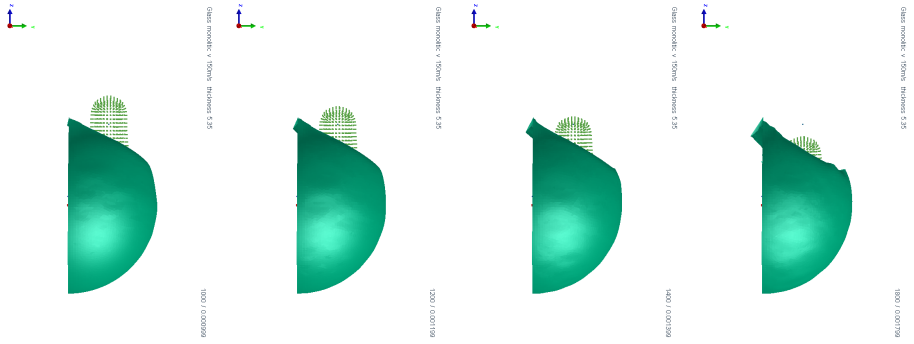

(e) t= 10 ms (f) t= 12 ms (g) t= 14 ms (h) t= 18 ms

Figure 4.11: Collapse sequence for monolithic bubble (t=5 mm) at 150 m/s

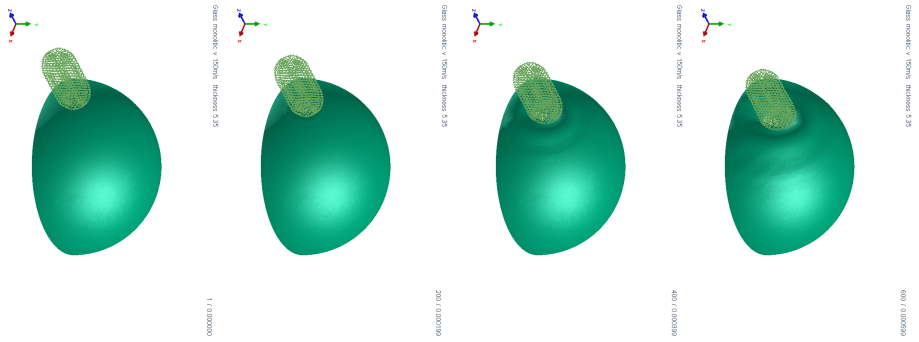

(a) t= 0 ms (b) t= 2 ms (c) t= 4 ms (d) t= 6 ms

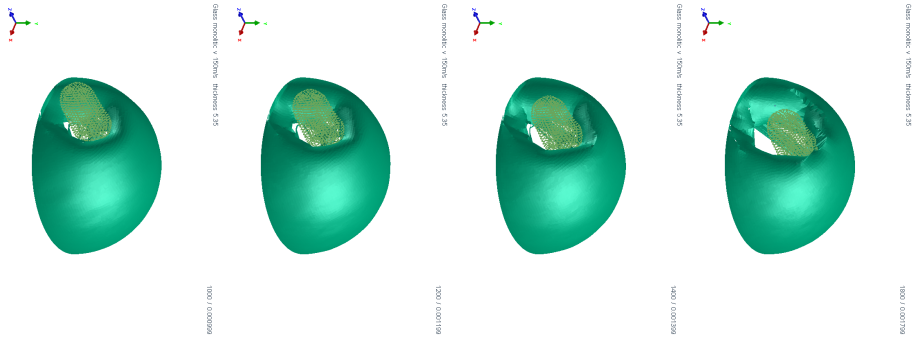

(e) t= 10 ms (f) t= 12 ms (g) t= 14 ms (h) t= 18 ms

Figure 4.12: Collapse sequence for monolithic bubble (t=5 mm) at 150 m/s (Isometric view)

Chapter 5

Further Studies And Concluding Remarks

"The more I think of it, I find this conclusion more impressed upon me — that the greatest thing a human soul ever does in this world is to see something, and tell what it saw in a plain way"

- John Ruskin, *Modern painters*

5.1 Further Studies

After the whole analysis was performed, some areas of improvement for future studies related with the present work have been found. This chapter shows that areas that would ameliorate the model and will produce an accurate approach to the problem.

The following suggestions are devoted to the optimization of the structure, model and results obtained. These suggestions regard to boundary condition definition, temperature effect, bubble design and test validation.

To end up, the key ideas of the whole research are collected.

5.1.1 Boundary condition definition

Once the different analyses have been performed, the failure of the model at critical speed in boundary conditions was noticed.

The definition of such conditions in this analysis (constraining all degrees of freedom simulating a clamped boundary) was very simple since the results needed were valid although the B.C would fail. However, the design of a suitable mounting and supporting boundary structure for an impact resistant structure would allow an accurate approach. The windshield frame should have sufficient stiffness to transmit the imposed loads without serious deformation, and it would be very interesting for further studies the investigation of those loads transmitted to the aircraft fuselage.[33]

Therefore, it would be engaging the implementation of a more realistic boundary condition as a C-shaped frame shown in figure 5.1. This new boundary will fix every translational and rotational degree of freedom of the surround

contour in the same way than the one already used, but it would provide flexibility to the model. However, this implies the definition of a new part and the corresponding attachment to the transparency. The attachment must be correctly defined and, in order to be realistic, a model of the real bolts must be introduced in the FE model.

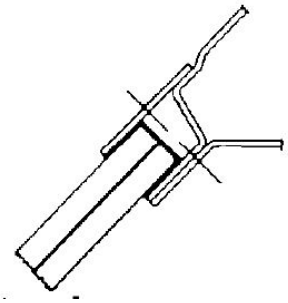

Figure 5.1: C-shaped frame[33]

The use of bolts typically employed in the attachment to the fuselage is a feature to be concerned about. These bolts could produce a concentration of stress in the holes which will be followed by an initial failure and crack propagation.[34]

Consequently, the definition of a realistic boundary condition would provide a lot of close to real structure behaviour results, but its definition must be carefully established.

5.1.2 Temperature effect

Previously, it was stated that aircraft's transparencies use acrylic polymers, which are materials very sensitive to temperature. For the bird impact resistant design, the mechanical properties and the different influence factors are important features to take into account.

A lot of investigations have demonstrated the heavy dependence on temperature of those kinds of materials, but focusing on mechanical and dynamic properties, the results have shown that [35]:

- Quasi-static loading: The increment of temperature has two effects: the Young's modulus decreases and at the same time this produces a decrement of the flow stress. As consequence, the plastic strain increases.

- Dynamic loading: The temperature effect on the mechanical behaviour was notable in this case. As temperature increases, the failure strain increases, leading to a decrement of the failure stress. It is remarkable that at temperature near glass transition temperature, the materials do not fail after huge plastic deformation.

Also, this influence should be taken into account in the frame and fasteners, where the transparency would be allocated. Fasteners must permit expansion and contraction, as the frame should be sufficiently extensible to allow thermal expansion.[35]

So for a more comprehensive determination of the material properties, a further study may be done on the temperature dependency of the material.

5.1.3 New Observation bubble design

It has been checked that the monolithic design of the observation bubble behaves worst than a laminated model. The laminated model is able to resist higher impacts reducing the weight of the transparency. As it is well-known, weight is always a feature to be concerned in the aeronautic field, and then the reduction of it is always an advantage.

On the other hand, the creation of the bubble geometry with the laminated model is more complicated and more expensive.

Therefore, an analysis of a new laminated design would produce much better results. In this line of thought, a study of the material used in the interlayer and external layers would improve the results in the same way that the increment of number of layers could give some advantages to the model.

Similar studies were performed by *the Hesa Institute for Aeronautical Research of the Isfaham University of Technology* [16]. Those studies validated with experimental results showed that the three-layer construction, with two cast acrylic layers and a PVB interlayer, provided the best results. This model was able to have a limit speed of 79.2 m/s showing good strength. Regarding materials, the numerical results showed that if the modification is properly done, the bubble would be able to improve its behaviour. For that purpose, PU (Polyurethane) is proposed since it was checked that this interlayer was completely safe during the impact avoiding the penetration of the bird.[16]

5.1.4 Test validation

Due to the huge cost of experimental tests, these researches based on numerical simulations are required. But in order to have a complete validation, experimental tests are needed. This is why the final validation of the model will be through the comparison of results with experimental data. Since this data is not already available, the realization of experimental test to check and validate the model would be useful.

In that way, it would be possible to prove the validation of the structure to satisfy the bird-strike requirement according to CS-25 and FAR-25. Besides, the implementation of the new laminated structure would be checked.

Appendix B shows an estimation of the cost needed to perform the required tests to validate the results. It can be compared with the budget obtained for the project in Appendix A. It is clear the huge difference between both budgets, making evident the advantages of the realization of numerical simulations as first approaches.

5.2 Concluding Remarks

During all phases of this project several conclusions have been gathered and they are summed up as follows:

1. SPH is the most suitable numerical method to model bird strike. It has been checked against experimental data that this method, with a shape of a cylinder with hemi-spherical ends, produces results very close to reality.

2. The importance of the definition of target material. Since transparent materials have a high dependency on strain rates, its influence must be taken into account.

3. Mesh geometry helps to guide the pattern, so it is needed to pay special attention to it.

4. Material modelization:

   - Material type 143 does not work properly because the strain rate interpolation does not fit the real behavior of the material.
   - Material type 126 leads to large time step reduction (simulation error) associated with large deformations of damaged elements.

     A better modelization of transparencies materials is needed. As a future idea, the implementation of user defined material would be an optimal option.

5. Three-layer laminate model allows higher impact velocities reducing weight. Consequently, a bubble composed by three layers would allow higher impact velocities before failure.

6. The increase of thickness enhances the ballistic limit velocity. On the other hand, as thickness increases, weight does as well. The laminated model would be a possible solution finding the perfect balance between both characteristics.

Appendices

Appendix A

Project Budget

This appendix shows the global cost needed for the performance of this research.

The performance of this project started on February and it has finished on June of 2015. The first three months, the project was done during an internship in the department of Structural Dynamics and Aeroelasticity at Airbus Defence and Space (Airbus Group). The project can be divided into several stages:

- **Familiarization with the different computer programs, getting started**: The time of the first two weeks was used to learn and acquire the basic skills needed to develop the work. In order to perform the bird impact numerical simulation 'Visual-Performance Solution'(formerly PAM-CRASH) was learned. At the same time, a detailed investigation on the bird strike problem, relevance and literature survey on bird strike numerical simulation was done.
- **Characterization of the bird**: The characterization of the bird is one of the main tasks, since the good behaviour of the model depends heavily on its definition. This is why five weeks were spent on this labour.
- **Modelization of the transparency**: After the definition of the bird, the next five weeks were used to develop a transparency model which simulates a typical windshield. In these five weeks, a deep analysis based on different materials and meshes was carried out.
- **Simulation of bird strike in semi-spherical transparencies**: Once the bird and the transparency models are already designed, the semi-spherical shape was integrated in a FEM during the three following weeks.
- **Further work**: A complete revision of the work performed was done in order to sum up the characteristics of the research that would be optimized for further studies. For this fact, one week was spent.
- **Documentation of all previous results**: After the collection of the most important results, they were documented. This process must be done carefully comparing the numerical results with the available test and literature results. This is why four weeks were spent.

The following tables gather the project budget needed for the performance of this research. Table A.1 shows the different phases of the project with an

estimation of the spent time in each one. Consequently, it is deduced that the time spent for the project is 960 hours, 60 of which have been shared with the tutor, increasing to a total of 1020 hours. Notice that the hours per week spent are of the order of 8 per day.

	Definition	**Weeks**	**Hours**
Phase 1	Getting started	2	96
Phase 2	Characterization of the bird	5	240
Phase 3	Modelization of the transparency	5	240
Phase 4	Semi-spherical transparencies	3	144
Phase 5	Further work	1	48
Phase 6	Documentation	4	192
Total		20	960

Table A.1: Project phases

Based on Airbus Defence and Space remuneration, a salary of 45€/h for the senior engineer and a salary of 17 €/h for the intern was established, obtaining a personal cost of 19,020 €.

Concept	**Price(€)**	**Amortization**	**Final price** (€)
Computer	1,000	1/4	250
PAM-CRASH Software	25,000	1/3	8,333
ABAQUS Software	25,000	1/3	8,333
MATLAB Software	4,000	1/3	1,333
Documentation	-	-	90
Total			18,340

Table A.2: Equipment and software licenses costs

In table A.2 an itemization of equipment and software licenses costs are collected. An amortization coefficient based on 2015 rates has been applied to take into account the depreciation of the different elements, obtaining a total price of 18,340€.

Finally, including the indirect cost assumed as 20% of the global one, as table A.3 shows the total cost is 44,832€.

Concept	**Total cost(€)**
Personnel	19,020
Equipment and Software licenses	18,340
Indirect costs (20%)	7,472
Total	**44,832**

Table A.3: Project Budget

Appendix B

Validation tests budget

This appendix contains an estimation of the required budget that would be necessary to validate the numerical results obtained in this research. The experimental test is divided into three stages:

1. **Target flexibility influence**: The targets used will be completely rigid. As it is typical because of its low price, aluminium will be the material used. The impacts will be performed on three different plates varying its thickness (0.8 mm, 3 mm and 15 mm) but keeping the same dimensions (0.7m x 0.7m). On each plate, a 4 lb bird will impact at three different speeds (100, 150 and 200 m/s).Every test will be repeated to check the consistency of the results three times. Besides, the experiment will be done at two inclinations: 90° and 45°. The measurement equipment is composed of computer to digitalize all data, and pressure transducers mounted on the plate to provide the pressure time history during the impact event.

2. **Characterization of the transparency**: In this case, each transparent target cannot be reused consequently the test can only be done once. A similar plate in terms of dimensions and thickness than the numerical simulation is used (0.7 x 0.7m and 5.3 mm), being PMMA the material of the target. Two inclinations and different speeds: 25, 50, 100 and 150 m/s will be the changes for the impacts. Three identical launches will be done,needing a specific transparency for each one;needing a total of 24 targets. The measurement equipment is only composed of a high speed camera to obtain the collapse sequence.

3. **Bird impact on bubbles**:

   Bubbles of PMMA are not reusable and due to its high price, only three tests can be done without repetitions.Three birds at 50, 100 and 200 m/s will be launched; consequently, three bubbles are needed.

For this end, some prices estimations have been calculated as it is shown in the following tables. The table B.1 contains the cost of the material employed for the different targets. Secondly, table B.2 gathers the equipment price applying an amortization coefficient according to depreciation tables of 2015.

Material					
Phase	**Material**	**Thickness(mm)**	**Price**	**Units**	**Total cost(€)**
Rigid Plate	Aluminium	0.8	1.7€/kg	12	21.72
		3.0		12	81.72
		15.0		12	406.8
Flat transparency	PMMA	5.3	15.45€/kg	24	370.85
Bubble	PMMA	5.3	10,000€/piece	3	30,000
Total	-	-	-	-	30,881.09

Table B.1: Experimental project phases

Equipment			
Description	**Price (€)**	**Amortization**	**Total cost(€)**
Pressure transducers	1,000	1/4	250
High Speed Camera	50,000	1/4	12,500
Computer	1,000	1/4	250
Launcher	12,000	1/4	3,000
Other costs	200	-	200
Total	-	-	16,200

Table B.2: Equipment costs

The table B.3 shows the cost applied to the realization of the different bird strikes. The most relevant data is the high price of the first strike (12,000€) due to the whole set up needed. Once the first specimen is launched, the other strikes reduce their cost a 90%, i.e. 1,200€.

Bird strike performance			
Number of impacts	**Impact price (€/impact)**	**Bird price(€)**	**Total cost (€)**
1	12,000	5	12,005
80	1,200	5	96,400
Total			108,405

Table B.3: Bird strike performance costs

Finally, the table B.4 presents the final budget required to perform the whole set of tests. The budget comes to 160,526.09€.

Concept	**Total cost(€)**
Personnel	5,040
Material	30,881.09
Equipment	16,200
Bird strike performance	108,405
Total	**160,526.09**

Table B.4: Project Budget

Appendix C

Rigid Target Results

The figures C.1 and C.2 show the experimental pressure variation on the different pressure gauges on the target, as picture 2.7 depicts, and the numerical results obtained from the simulations.

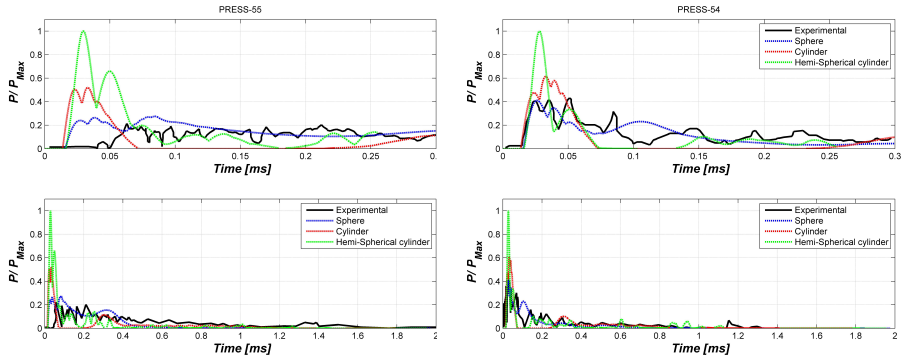

(a) PRESS 55

(b) PRESS 54

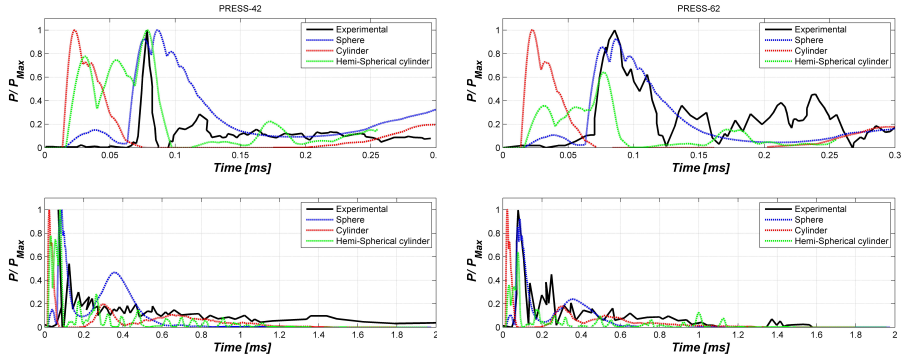

(c) PRESS 42

(d) PRESS 62

Figure C.1: Variation of shape: pressure

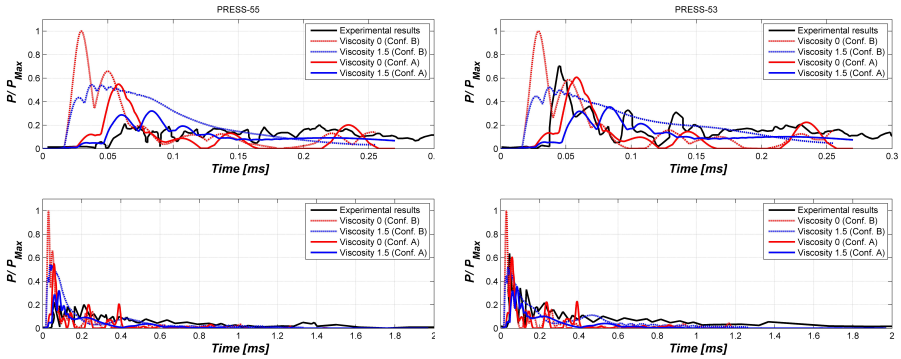

(a) PRESS 55 (b) PRESS 53

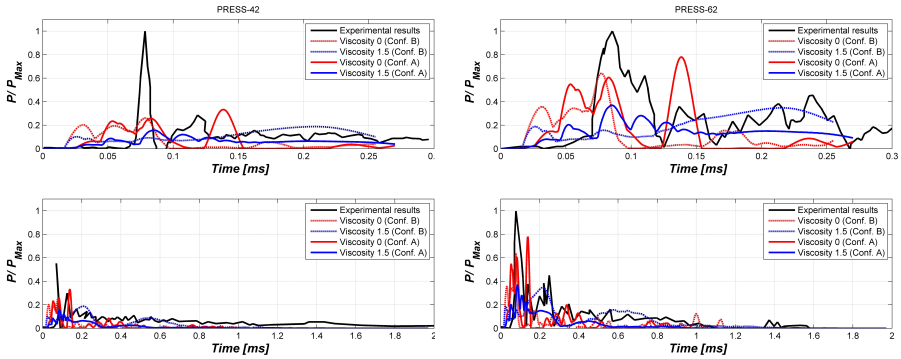

(c) PRESS 42 (d) PRESS 62

Figure C.2: Configurations' pressures

Bibliography

[1] Ilias Maragakis. Bird population trends and their impact on aviation safety 1999-2008. *European Aviation Safety Agency*, 2009.

[2] Science & AAAS[1]. Blue lights could prevent bird strikes, March 2015. `http://news.sciencemag.org/plants-animals/2015/04/blue-lights-could-prevent-bird-strikes`.

[3] James S Wilbeck. Impact behavior of low strength projectiles. Technical report, DTIC Document, 1978.

[4] Jukka-Pekka Nikolajeff. *Analysis of the Bird Strike Reports Received by the Finnish Transport Safety Agency between the Years 2000 and 2011.* PhD thesis, Cranfield University, 2014.

[5] Safety Regulation Group. Large flocking birds. An International Conflict Between Conservation and Air Safety. Technical report, Safety Regulation Group Civil Aviation Authority, 2000.

[6] Airbus Defense & Space. C295 the tactical warehouse. `http://militaryaircraft-airbusds.com/aircraft/c295/c295about.aspx`, March 2015.

[7] L.Benítez Montañes and J.L Pérez-Galán. Academia: Bird strike numerical simulation-mt-pr-140010. Technical report, Structural Dynamics and Aeroelasticity Department. Airbus Defense and Space, 2014.

[8] Alexander Krastev. EASA Regulatory Instruments, February 2015. `http://www.skybrary.aero/index.php/EASA_Regulatory_Instruments`.

[9] Certification Specification EASA. Certification specifications for large aeroplanes CS-25. Technical report, Tech. Rep. Amendment 3, European Aviation Safety Agency, 2007.

[10] Paul J Callus. DEF STAN 00-970 requirements for the design and airworthiness of composite aircraft structure. Technical report, DTIC Document, 2003.

[11] Michele Guida. *Study Design and Testing of Structural Configurations for the bird-strike compliance of aeronautical components.* PhD thesis, Università degli Studi di Napoli Federico II, 2008.

[1] Advancing Science, serving society

[12] Lakshmi S Nizampatnam. *Models and methods for bird strike load predictions*. PhD thesis, Wichita State University, 2007.

[13] Sebastian Heimbs. Computational methods for bird strike simulations: A review. *Computers & Structures*, 89(23):2093–2112, 2011.

[14] ESI Group. Visual-environment, March 2015. `https://www.esi-group.com/es/software-services/virtual-integration-platform/multi-domain-simulation/visual-environment`.

[15] Aaron J Siddens, Javid Bayandor, and Frank Abdi. Soft impact damage prognosis of F-16 canopy using progressive failure dynamic analysis. *Journal of Aircraft*, 51(6):1959–1965, 2014.

[16] H Salehi, S Ziaei-Rad, and MA Vaziri-Zanjani. Bird impact effects on different types of aircraft bubble windows using numerical and experimental methods. *International Journal of Crashworthiness*, 15(1):93–106, 2010.

[17] John P Barber, Henry R Taylor, and James S Wilbeck. Bird impact forces and pressures on rigid and compliant targets. Technical report, DTIC Document[2], 1978.

[18] ESI Group. Virtual performance solution 2010 solver notes manual. Technical report, ESI Group, 2010.

[19] Gui-Rong Liu and Moubin B Liu. *Smoothed particle hydrodynamics: a meshfree particle method*. World Scientific, 2003.

[20] N Dennis and D Lyle. Bird strike damage & windshield bird strike final report, 2008.

[21] William R Pinnell. Frameless transparencies for aircraft cockpit enclosure, April 5 1988. US Patent H451.

[22] John Bohannon. Bird Strike Research Suggests DNA Technique Can Help Stop Bird-Airplane Collisions, February 2013. `http://www.huffingtonpost.com/2013/12/15/bird-strike-dna-birds-crashing-planes_n_4441422.html`.

[23] Steve. Bird strikes. no laughing matter..., February 2009. `http://www.roger-wilco.net/bird-strikes-no-laughing-matter/`.

[24] Christopher Neiger. How automotive glass works, 2009. `http://auto.howstuffworks.com/car-driving-safety/safety-regulatory-devices/auto-glass2.htm`.

[25] LH Abbud, ARA Talib, F Mustapha, H Tawfique, and FA Najim. Behaviour of transparent material under high velocity impact. *Int. J. Mech. Mater. Eng*, 5:123–128, 2010.

[26] Mark Gevers. Advanced laminated glass modeling for safety fea tecosim internal research project. Technical report, TECOSIM Technische Simulation GmbH, 2011.

[2] Defense Technical Information Center

[27] Erke Wang, Thomas Nelson, and Rainer Rauch. Back to elements-tetrahedra vs. hexahedra. In *Proceedings of the 2004 International ANSYS Conference*, 2004.

[28] Sai Sarva, Adam D Mulliken, Mary C Boyce, and Alex J Hsieh. Mechanics of transparent polymeric material assemblies under projectile impact: simulations and experiments. Technical report, DTIC Document, 2004.

[29] Martin Larcher and George Solomos. Laminated glass loaded by air blast waves–experiments and numerical simulations. *Joint research centre technical note, Pubsy JRC57559*, 2010.

[30] PA Hooper, BRK Blackman, and JP Dear. The mechanical behaviour of poly (vinyl butyral) at different strain magnitudes and strain rates. *Journal of Materials Science*, 47(8):3564–3576, 2012.

[31] Colin Morison. *The resistance of laminated glass to blast pressure loading and the coefficients for single degree of freedom analysis of laminated glass.* PhD thesis, Cranfield University, 2010.

[32] Airbus Defense & Space. C295 search and rescue:the prove, reliable and low risk solution, May 2015. `http://c295.ca/resources/multimedia-library/search-and-rescue-sar/`.

[33] Pell Kangas and George L Pigman. Development of aircraft windshields to resist impact with birds in flight (part ii): Investigation of windshield materials and methods of windshield mounting. Technical report, SAE Technical Paper, 1948.

[34] Arcangelo Grimaldi. *SPH High Velocity Impact Analysis. A Birdstrike Windshield Application.* PhD thesis, University of Naples Federico II, 2011.

[35] Hong Yu Fei Xu Zhongbin Tang Lei Li Tao Suc, Yulong Li. Temperature effect on the mechanical behavior of acrylic polymers under quasi-static and dynamic loading. *Composites: Mechanics, Computations, Applications: An International Journal*, 5(3):195–205, 2014.